Pluto Hop, Skip, and Jump

NIAC Phase II

Final Report

For the period 17 June 2021 – 8 September 2023

Prepared by

Kerry T. Nock (PI), Derek Lo, and Mark Warnecke
Global Aerospace Corporation

Dr. Jamey D. Jacob (Co-I) and Kathleen McNamara
Oklahoma State University

Dr. Karl L. Mitchell (Co-I) and Dr. Jason Hofgartner (now with SwRI),
Jet Propulsion Laboratory

8 September 2023

Grant Number: 80NSSC21K0956

GAC Report: 510-K0956-005

This version of the Final Report is suitable for public release.

Oklahoma State University Participants

Dr. Jamey D. Jacob (Co-I) – Professor and Director of the Unmanned Systems Research Institute (USRI)
Dr. Hadi Noori – Professor and Director of the Lightweighting Research Center
Kathleen McNamara - Research Engineer
Ben Loh - Assistant Research Professor
Alvin Ngo – Graduate Research Student
Leo Fagge - Undergraduate Research Student
Student Capstone team: Travis Pilati, Leesha Gillilan, Graham Tyra, Dalton Reese

Executive Summary

This is the Final Report from Global Aerospace Corporation for this NIAC Phase II effort (Grant No.: 80NSSC21K0956 to develop the Pluto Hop, Skip, and Jump mission concept. The possibility is discussed of using the tenuous atmosphere of Pluto to slow down from 14 km/s to about 0.1 km/s using an Enveloping Aerodynamic Decelerator (EAD), a new technology for entry, descent, and landing (EDL). EDL and propulsive technologies are discussed along with EAD envelope concept; thermal design; envelope seam design; packing and deployment testing; and envelope component thermal and load testing. Also summarized are the mission concept of operations, and landing zone uncertainty analysis results.

Global Aerospace Corporation and its research partners, Oklahoma State University (OSU) and the Jet Propulsion Laboratory (JPL), have documented in this final report the status of the Phase II work during the contract period (17 June 2021 – 8 September 2023). Key accomplishments include:

- Document mission science motivation and initial look at lander science packages,
- Completed a Monte Carlo analysis of error components that go into landing site uncertainty at Pluto indicating the EAD is feasible regarding landing site uncertainty,
- Completed initial study of EAD-enabled Triton lander mission modes that include direct entry from interplanetary hyperbolic tractor and a secondary payload option from a Neptune flagship orbiter mission,
- Began the development of two new EAD technology spin-offs including a space station crew rescue pod and a neutral atmospheric density monitoring system.
- Fabricated several 1/20th scale model EAD envelopes for packing, deployment, and inflation tests and conducted packing and inflation experiments,
- Completed the analysis of the membrane stress on the envelope during peak heating and inertial loading,
- Conducted laminate breaking stress testing at room temperature,
- Completed a refined thermal analysis of the Pluto EAD envelope and gas temperatures,
- Designed and conducted experiments on several envelope gore seam design concepts, and
- Briefed key NASA technologists and the OPAG on the concept and EAD technology.

Table of Contents

TABLE OF FIGURES

TABLE OF TABLES

1 Introduction

New Horizons (NH) was traveling at 14 km/s when it flew past Pluto. If it had been desired to land a payload on the surface using propulsion, it would have needed a three-stage retrorocket. This would have required almost all its mass to be converted to propellant. It could have landed perhaps 1 kg of payload. It is expensive to slow down that much propulsively. A future Pluto lander mission would need a very large propulsion system at Pluto and, as a result, a much larger, more expensive launcher at Earth. Alternatively, a spacecraft could include a nuclear, low-thrust propulsion system to get to Pluto quickly and slow down to make the landing propulsion system practical; however, this would be very expensive and beyond the cost bounds of a NASA New Frontiers mission.

The key challenge of the Pluto Hop, Skip and Jump mission is slowing down from a fast interplanetary approach speed and landing on a planet with very little atmosphere and doing so with a low-cost system. For a short flight to Pluto (11 years) the approach speed is about 14 km/s, about twice as fast as low Earth orbit speed. To make matters worse, the Pluto atmosphere is only about 1/100,000th of Earth surface pressure. So, how can we land given these conditions with a low-mass, low-cost project? If we meet this challenge, we could do a Pluto lander mission with a similar budget to NASA's NH Mission. A key solution to meeting this challenge is Enveloping Aerodynamic Decelerator (EAD) technology. Figure 1 illustrates one concept of operations for the Pluto Hop, Skip and Jump mission.

In the initial phase of the Phase II effort, we reestablished the importance of the Pluto mission in relationship to the key New Horizon's mission findings and the 2013-2022 Decadal Survey themes. In addition, we began to address the three main system challenges, which are the Pluto landing uncertainty using EAD technology, the EAD envelope packing, deployment, and inflation; and the strength of the envelope given the Pluto entry thermal and loads environment.

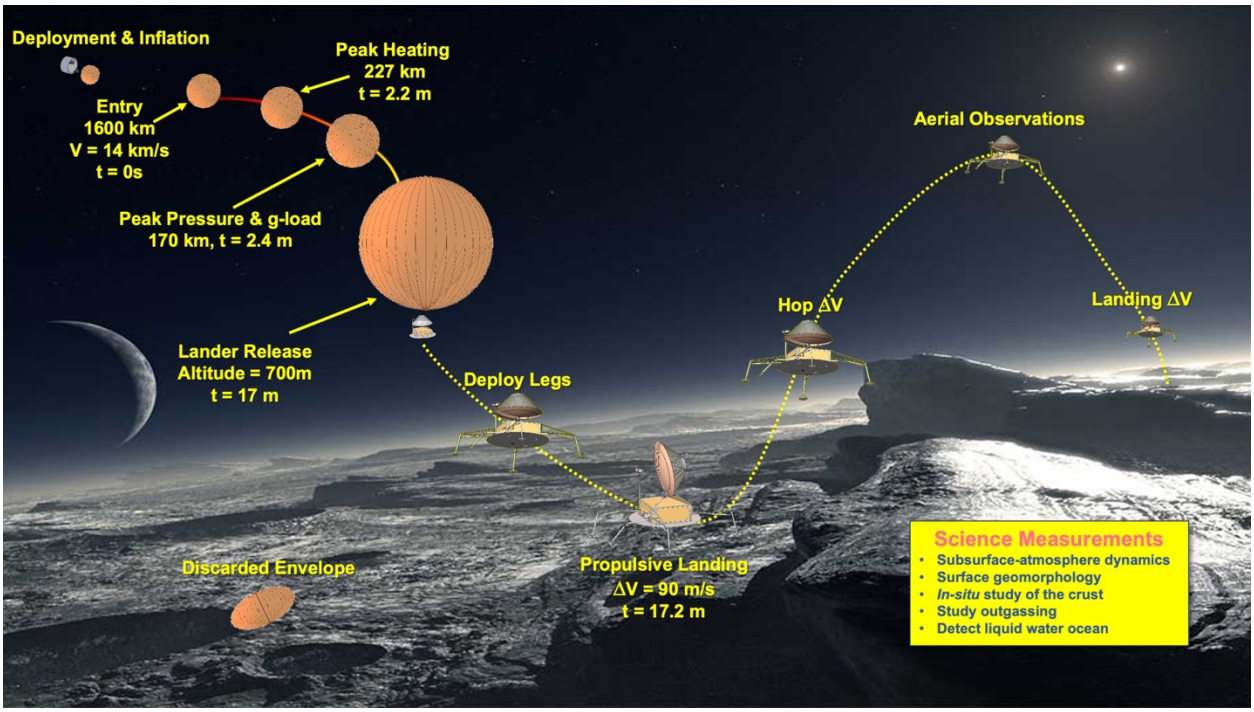

Figure 1. Concept of operations.

2 Science

In this section we discuss the New Horizons mission unexpected findings, the most recent National Academies Decadal Surveys, interest in Triton as another possible EAD mission candidate, and potential lander science instrumentation.

2.1 New Horizons Pluto Mission: Unexpected Findings

Since the flyby of NASA's New Horizons (NH) spacecraft in 2015, Pluto has attained considerable scientific attention as a very exciting Kuiper Belt Object (KBO). Some key unexpected findings from the New Horizons Mission are the a) complexity of Pluto and Charon, one of its five satellites, b) recent and ongoing activity on its surface, c) significantly lower-than-predicted atmospheric condensation rate, and d) evidence for an internal water ocean. These discoveries have intensified scientific interest in the Pluto-system and Kuiper belt and motivated interest in further exploration by future orbiters and landers, which is exemplified by NASA's selection of Pluto and Triton mission concepts studies to support the Decadal Survey effort.

2.2 Decadal Survey

Every ten years, NASA's Planetary Science Division (PSD) and the National Science Foundation (NSF) calls upon the National Academies to:

1. Assess the status of an entire scientific discipline,
2. Identify key scientific questions to be addressed in the next decade,
3. Prioritize the most important initiatives to address these questions,
4. Provide Technical Risk and Cost Evaluation (TRACE) for recommended projects/missions, and
5. Conduct independently by the National Academies for sponsoring agencies.

2.2.1. Past Themes

There were three high-priority Decadal Survey cross-cutting science themes of the last survey (2013-2022). These included *Formation*, *Habitability*, and *Workings*. The Pluto lander mission addresses all three of these cross-cutting science themes.

The Pluto system records physical and chemical properties of the Kuiper belt, the Solar System, binary systems & giant impacts. Measurement of the atmosphere and surface isotopic ratios would strongly constrain the chemical properties of the Kuiper belt (*formation*).

Pluto has complex organic chemistry abundant in hazes and measurable tholins, which are organic substances effected by UV radiation; and a possible subsurface ocean and cryovolcanism. Assessment of complex organics in the atmospheric hazes and surface tholins is important for understanding the habitability of this candidate Ocean World (*habitability*).

We note that the processes on Pluto are diverse, unique, and ongoing. High-resolution, time-elapsed imaging of surface-atmosphere exchange by sublimation and condensation enables further quantification of these dominant ongoing processes (*workings*).

So, under past Decadal Survey, the Pluto system, and Pluto as a representative KBO, offers fundamental and unique contributions to all three priority themes.

2.2.2. Latest Survey

The recently released Decadal Survey, entitled, ***Origins, Worlds, and Life: A Decadal Strategy for Planetary Science and Astrobiology 2023-2032***, has many references to Pluto and Triton. The latest Decadal Survey report for 2023-2032*, was released in 2022.

There were 12 priority science questions in the decadal survey that possibly relate to future Pluto and Triton exploration. Of these Pluto and/or Triton exploration could contribute to 7 of the 12 priority questions.

In addition, the survey recommended a Triton Ocean World Surveyor (TOWS) mission for New Frontiers 7 opportunity. An EAD could enable a Triton orbiter or lander for this mission.

The survey also found that NASA and the science community could benefit from studying aerodecelerator technologies, like EAD, that could be integrated into future missions to increase science value.

2.3 Triton

In addition to a fast, inexpensive Pluto Lander mission, EAD technology ***could enable a lander on Triton***. Triton, the largest moon of Neptune, is a Pluto-like body with similar mass, size, surface composition and atmosphere. Triton is of particular scientific interest because of its retrograde orbit, indicating it was captured and possibly originated from the Kuiper belt. Triton was identified as the highest priority candidate ocean world to target in the near term by the NASA Roadmap to Ocean Worlds. In addition, during the Voyager 2 encounter in 1989, active geysers were observed along with over a hundred dark streaks likely from former geyser eruptions. Triton's similarity to Pluto makes it conducive to entry decent and landing (EDL) by ultra-low ballistic coefficient EAD technology.

2.4 Lander Science Instrumentation

In this section we discuss proposed landed science instruments for Pluto or Neptune's largest moon Triton. High heritage instruments for icy world landers are limited since the only lander of an icy world was the ESA Huygens, which is very old technology. We have assumed the use of Mars instruments or, more typically, instruments being developed for the Europa Lander (at TRL 5-6). Not all of these instruments have available power requirements. These instruments appear to be within family for an approximate 20 kg payload.

2.4.1. Atmosphere Mass Spectrometer

A small, high performance Quadrupole Ion Trap Mass Spectrometer (QITMS) has been developed by JPL for multiple mission concepts. The JPL QITMS is currently the smallest flight mass spectrometer available for possible use on planetary descent probes as well as small bodies, including comet landers and surface sample return missions. It masses at 7.5 kg, has a volume of 7 liters, and requires about 8 W of power. This instrument would measure atmospheric species including isotopes, noble gases. The QITMS can make measurements of all required constituents in the mass range of 1–600 atomic mass units (u) at a typical speed of 50 mass spectra per second,

* National Academies of Sciences, Engineering, and Medicine 2022. Origins, Worlds, and Life: A Decadal Strategy for Planetary Science and Astrobiology 2023-2032. Washington, DC: The National Academies Press. https://doi.org/10.17226/26522. (Prepublication copy, May 6, 2022)

with a sensitivity of up to 1013 counts/mbar/sec and mass resolution of m/Δm = 18000 at m/q = 40† sufficient to resolve challenging species (e.g., N_2 from CO). The QITMS features a novel MEMS-based inlet system driven by a piezoelectric actuator that continuously regulates gas flow at inlet pressures of up to 100 bar. This mass spectrometer may require some minor modifications (e.g. a heater) to volatilize surface refractory ices, in addition to those in the atmosphere. It could be used upon descent in the atmosphere and periodically thereafter, hence its integrated power (energy) may be small.

2.4.2. Stereo Spectral Imager

The JHU/APL designed Europa Lander Stereo Spectral Imaging Experiment (ELSSIE) is a stereo and compositional imaging system developed for the Europa Lander. It is a 20-filter, 0.4-3.6 μm multispectral stereo imager. ELSSIE would: 1) provide panoramic and closeup views to support geological analyses; 2) collect visible and infrared data to identify and map enrichments in organics and non-ice phases; and 3) survey the landscape for spectral evidence of active surface processes. ELSSIE is 4.3 kg instrument, which is an overestimate for Pluto or Triton due to its Europa-specific radiation shielding. Does not need to be used continuously, so total integrated power (energy) is likely very small. It might be modified to expand spectral range out to 4.8-μm due to improve organics discrimination. It is actively being developed to TRL-6 under ICEE-2 Program. Other imaging options being explored includes a descent imager.

2.4.3. Seismometer

The Seismometer to Investigate Ice and Ocean Structure (SIIOS) is a small and efficient seismometer that was being developed by U. Arizona for Europa Lander, based on Silicon Audio COTS parts. Its mass is 300 g and requires about 120 mW of continuous power. It is also actively being developed to TRL-6 under ICEE-2 Program. A seismometer might not be as valuable at Pluto as Triton, since tides are very small (due to interactions with Charon), and impact fluxes and energies are poorly constrained.

2.4.4. Magnetometer and Atmospheric Pressure, Temperature and Wind Speed

The Mars Insight Lander Auxiliary Payload Sensor Suite (APSS) includes a tri-axial magnetometer, and neutral air sensors for pressure, winds, and temperature. The APSS mass is 568 g. The magnetometer component probably only valuable at Triton due to lack of driving field at Pluto. As flown on Mars Insight its TRL 9.

† the unit of m/q = u/e for the mass-to-charge ratio, where atomic mass unit and elementary charge are 1 u = 1.66×10^{-27} kg and 1e = 1.6×10^{-19} C, respectively

3 Pluto Flight System Design Summary

Most of this work on the system design was carried out during the Phase I effort, but in this section we include a brief description to provide context to the rest of the report.

3.1 Flight System Overview

Figure 2 illustrates an overview of the Pluto lander flight system we call an Entrycraft. That is, the flight system performs all the required functions from interplanetary cruise through to landing on Pluto. We will describe this system starting at the bottom right of this figure and going counterclockwise. During cruise, the lander systems function to provide communications and propulsive trajectory correction maneuvers. During cruise the Entrycraft is spin stabilized. On the top right, we illustrate a view of the Radioisotope Thermoelectric Generator (RTG) radiator, inflation tanks and envelope cover that are all jettisoned after envelope inflation reducing the flight system mass by about 260 kg. On the top left, is the fully inflated 70 m diameter envelope with the lander at the windward end. Internal load lines are shown that transfer the g-loads at peak acceleration into the EAD envelope at its equator. On the bottom left, is the 230 kg lander, that consists of structure, power, data handling, communications, propulsion, and science instrumentation systems. Note that the forward support structure is the EAD interface.

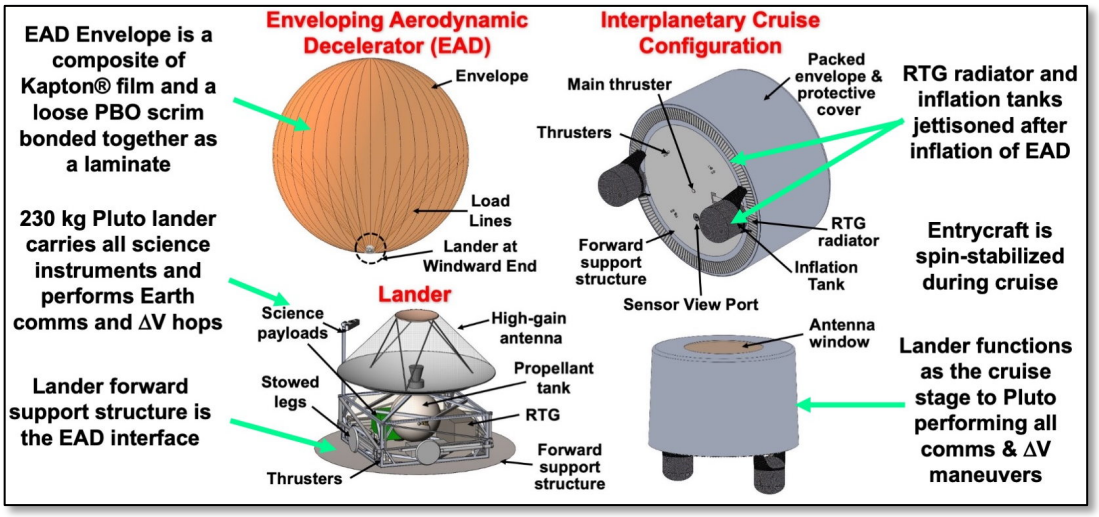

Figure 2 Pluto Lander *Entrycraft* flight system

3.2 Enveloping Aerodynamic Decelerator

The major benefits of an Enveloping Aerodynamic Decelerator (EAD) entry system are protection of the payload within the EAD and enabling the use of common film technology by keeping heating low. Entry stagnation point heating is two-orders of magnitude lower than conventional entry technology since the entry system has an ultra-low ballistic coefficient, which slows the entry vehicle high in the atmosphere where the density is low.

The EAD has an ultra-low mass to cross-section area ratio and since the EAD has a large nose radius the heating rate, which is inversely proportional to the square root of the nose radius, is also

very low. The thinness of the envelope and its high emissivity facilitates the escape of heat to cold space. The spherical shape eliminates embedded shocks and there are no shock impingements since the payload is enclosed within the decelerator envelope. Finally, this design uses conventional materials and eliminates need for traditional thermal protection systems (TPS).

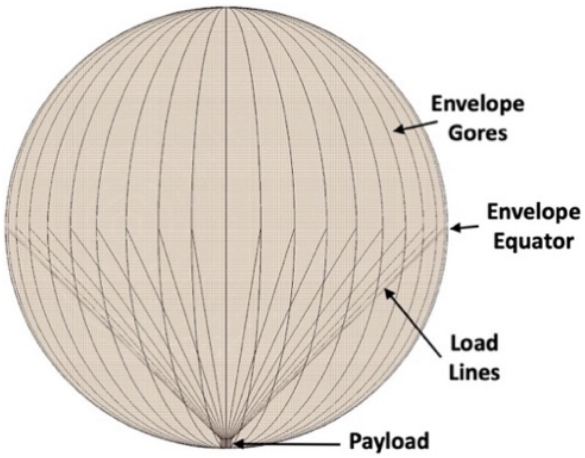

Figure 3 EAD envelope design showing payload support load lines

High-temperature shocks could be a major challenge for flexible and inflatable entry technology. However, EAD provides a solution by encapsulating the reentry payload within and at the windward end of the envelope, creating a uniform and stable, near-spherical surface without shock impingement to keep film and payload heating rates very low. So, with the payload within the envelope, both the envelope and payload are protected from shock heating.

Figure 4 is a schlieren image from a hypersonic wind tunnel test at the University of Texas, San Antonio (UTSA) illustrating the benign hypersonic shock geometry at Mach 7.2, which is similar to the Pluto EAD shock geometry at about 95 km altitude about 220s after entry.

For the Pluto mission, the EAD has a diameter of 70 m consisting of 96 major gores each made from 8 gore segments. The gore segments are fabricated from a two-function composite made of an ultra-thin polyimide film laminated to a polybenzoxazole (PBO) scrim. The film acts as a gas barrier while the PBO scrim handles loads due to deployment, membrane stress under internal pressure, and entry deceleration. The scrim is a weave with two different designs, a forward (ram-facing) region and an aft region (wake-facing). Load lines within the EAD envelope distribute the deceleration loads of the lander into the EAD envelope equator via a lightweight, fabric interface, which reduces loads in the ram-facing portion of the envelope where there is higher heating. The load lines also help keep the envelope shape spherical at the windward end of the EAD. The lander-hopper is initially installed within the envelope through a closeout feature. After entry and peak heating, and once the terminal velocity is low, the lander jettisons the EAD releasing it to land on the surface of Pluto.

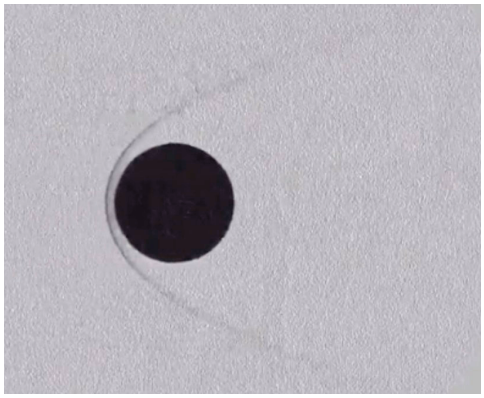

Figure 4 Schlieren image of a hypersonic sphere at Mach 7.2 (courtesy of Dr. Chris Combs at UTSA)

3.3 Cruise-Lander-Hopper

Prior to separation from the decelerator, lander-hopper performs all the functions of a typical cruise stage. It contains all the subsystems necessary for power, communications, propulsion and attitude control, and thermal control. After entry, and upon reaching terminal speeds just above the surface,

the lander-hopper is separated from the envelope, translated horizontally via thrusters away from the envelope, deploys its landing legs and configures its subsystems for the final main engine propulsive burn and landing. Figure 5 illustrates the lander-hopper on the surface of Pluto with its high-gain antenna pointed toward the Earth. The same main engine and thrusters are used to hop around the surface. Hopping is particularly efficient on Pluto since the gravitational acceleration is low, just 0.06 gee, and atmospheric drag at low speeds is negligible.

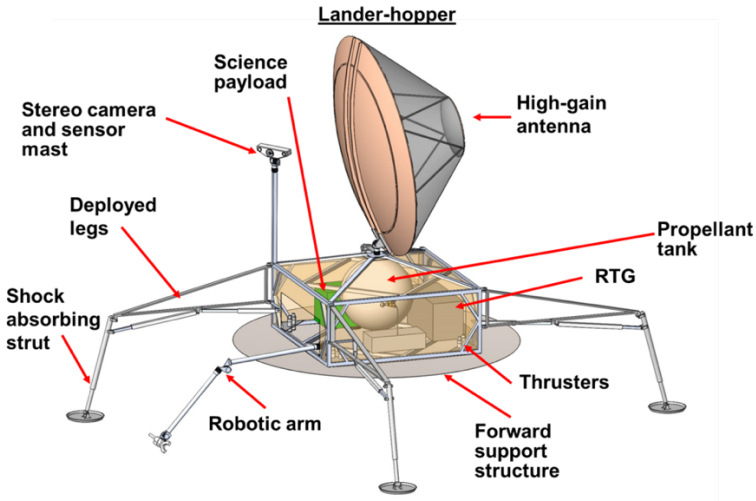

Figure 5. Lander-hopper conceptual design.

3.4 Hardware Jettisoned Prior to Entry

A thermal radiator, required to keep the lander-hopper cool during cruise, envelope inflation tanks, and the envelope outer protective cover are jettisoned after envelope deployment and inflation. The inflation gas is helium. A total of 20 kg of helium are required to inflate the envelope prior to entry. The tanks and plumbing for the helium are estimated to be 100 kg or about 5-times the mass of helium. The envelope micrometeoroid protective cover is estimated to be 20 kg. The RTG radiator is estimated to be 15 kg. Finally, we compute that up to 50 kg of propellant will have been used for trajectory correction maneuvers during the cruise to Pluto.

3.5 Entry System Mass Breakdown

Table 1 is a mass breakdown of the Pluto lander entry system. MEV is the Maximum Expected Value.

Table 1 Entry System Mass Breakdown

Component	MEV Mass, kg	Percent of EAD Mass
Gore Laminate Assy	303	73
Seams	92	22
Payload Support	22	5
Total EAD Mass	417	100
Lander Mass	230	-
Total Entry Mass	647	-

4 Mission Design Analysis

In the Phase II effort, the mission analysis consisted of studying the peak seam temperatures, envelope pressure, and hoop stress as a function of entry mass and EAD diameter; analyzing the Pluto lander dispersion given uncertainties in entry system, EAD aerodynamics, approach navigation, and atmospheric density; and exploring the use of EAD technology for landing on Neptune's large KBO-like moon, Triton.

4.1 Pluto Lander Mission Profile

An example Pluto Lander Mission is launched toward a Jupiter flyby on January 4, 2029 with Earth escape energy (C3) of about 117 km^2/s^2. The flight system, we call an Entrycraft, includes interplanetary cruise systems, EAD, and the Pluto Lander. Interplanetary trajectory correction maneuvers are performed periodically to keep the flight system aimed at Jupiter first and then at Pluto. About a year and a half after launch, the flight system performs a Jupiter gravity assist on July 2, 2030. Finally, after a little over eleven and a half years, the flight system reaches Pluto on September 11, 2040.

Figure 1, above, illustrates the Pluto Lander operations concept at Pluto after interplanetary cruise. In the top left of this figure, a 70-m diameter EAD envelope, with the 230 kg lander encapsulated at its windward end, is deployed, and inflated prior to entry. After inflation, it is beneficial to jettison heavy elements that are no longer needed, such as inflation tanks, envelope cover, and cruise power system heat exchanger making the flight system at least 260 kg lighter. Current best estimate (CBE)‡ of entry mass is 538 kg. Surface imaging through the forward sensor viewport begins prior to entry. The inflated EAD and payload enter the atmosphere at about 14 km/s with a nominal flight path angle (FPA) of -63.4° at a reference altitude of 1600 km followed by continuous deceleration to a terminal speed of about 90 m/s. Load lines within the EAD distribute the deceleration loads of the lander into the EAD envelope equator. Peak stagnation-point heating rates of about 3.63 W/cm^2 occur about 131 s into the entry at 236 km altitude. Peak g-load occurs about 143 s and is nominally about 29 gees. The EAD reaches a terminal velocity of about 90 m/s at about 700 m above the surface where the 230 kg lander then separates from the EAD envelope, deploys landing legs, and fires thrusters to translate away from the envelope and lands gently on the surface. Required landing propellant is less than 11 kg. The lander performs science measurements at the initial landing site and by firing the onboard thrusters, "hops" around the surface to investigate other scientifically interesting sites.

4.2 Reference Pluto Entry Conditions

As discussed above, the nominal flight path angle at entry is -63.4° and the speed is 14.01 km/s. Figure 6 displays the altitude and Pluto relative velocity versus time from entry. Figure 7 displays the velocity versus altitude and the Mach number versus time from entry. Figure 8 shows the flight path angle (FPA) and drag coefficient as a function of time from entry interface. Note the drag coefficient accounts for the various flight regimes including free molecular, transition and continuum. Figure 9 displays the heating rate (Sutton-Graves) and g-load as a function of time from entry. Figure 10 shows the dynamic pressure and Reynolds number versus time from entry. And finally, Figure 11 displays the Knudsen number as a function of time from entry.

‡ An entry mass of 640 kg is used for EDL thermal and loading analysis.

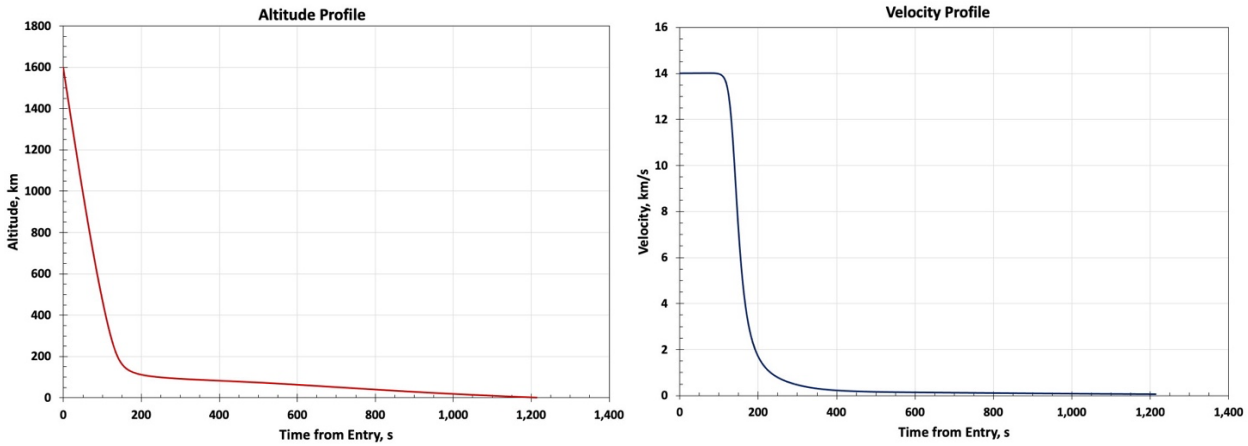

Figure 6 Nominal altitude and velocity as a function of time from entry.

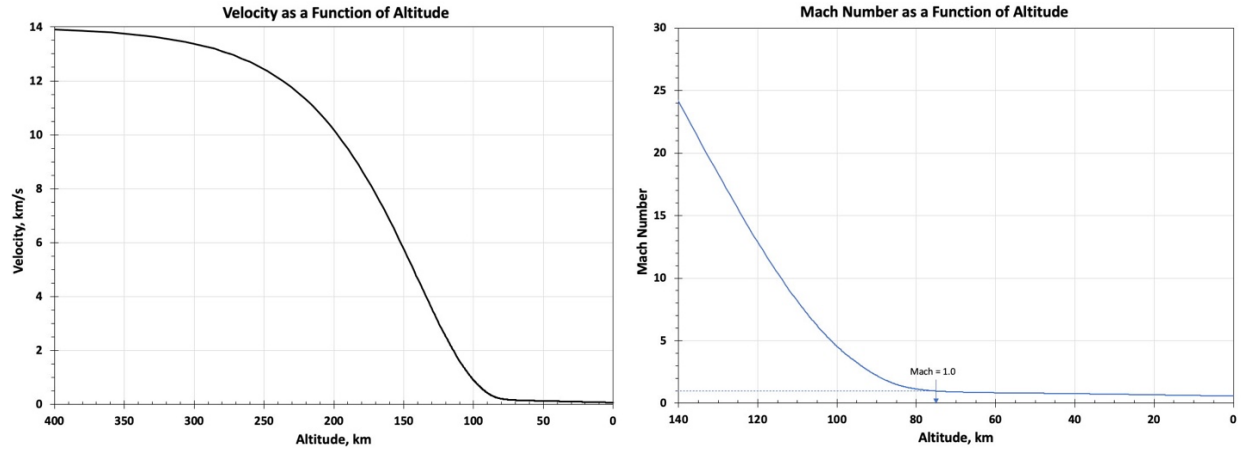

Figure 7 Nominal velocity vs. altitude and Mach number as a function of time from entry.

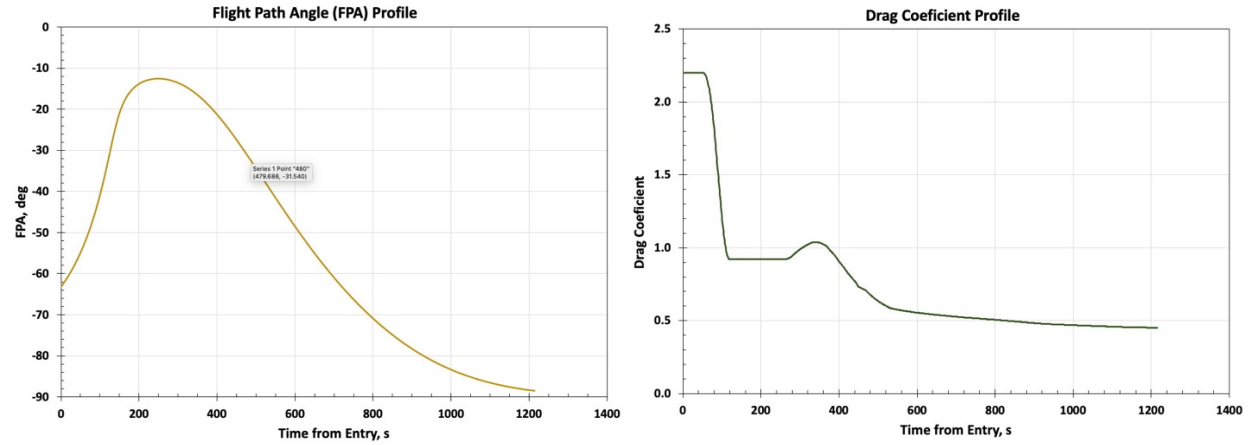

Figure 8 Nominal flight path angle and drag coefficient as a function of time from entry.

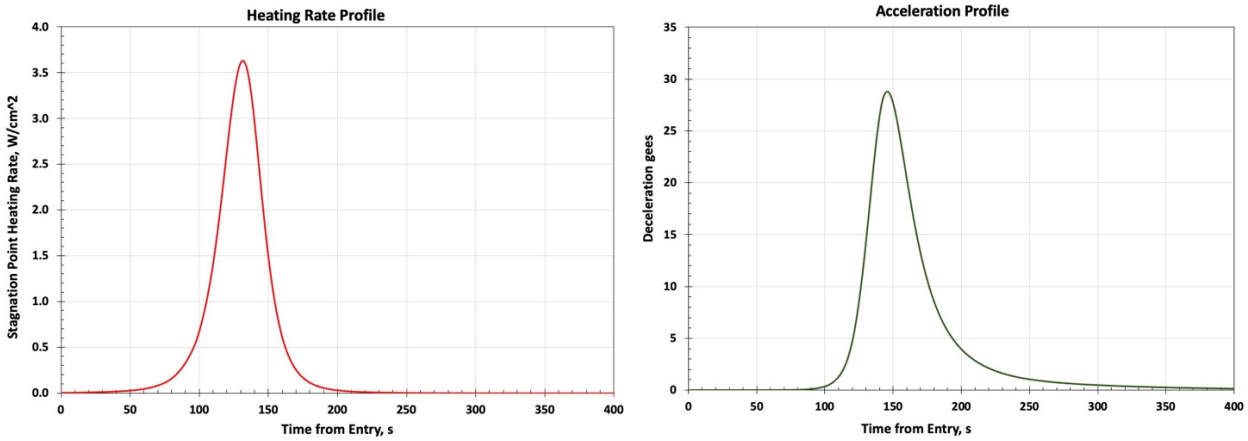

Figure 9 Nominal heating rate and acceleration as a function of time from entry.

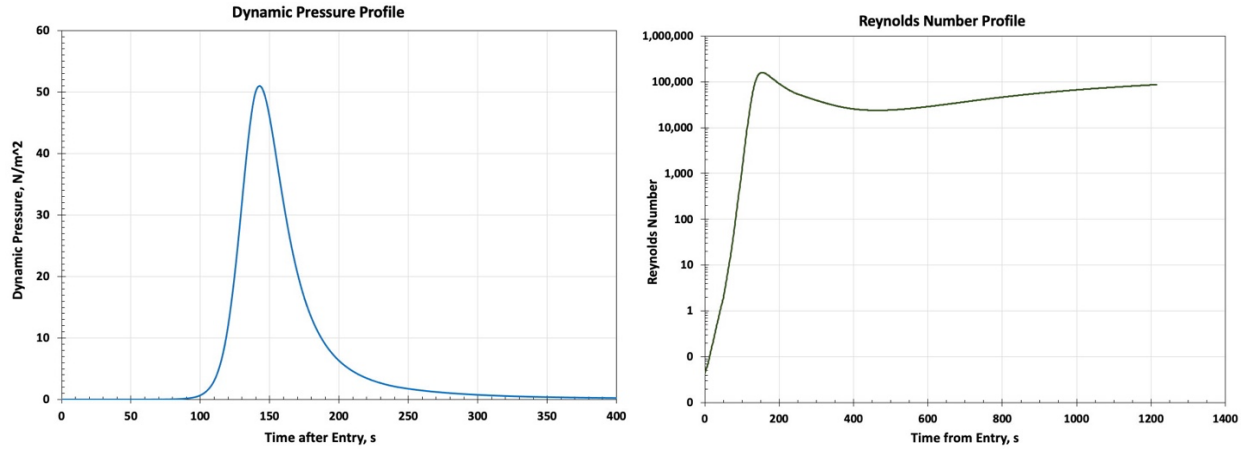

Figure 10 Nominal dynamic pressure and Reynolds number as a function of time from entry.

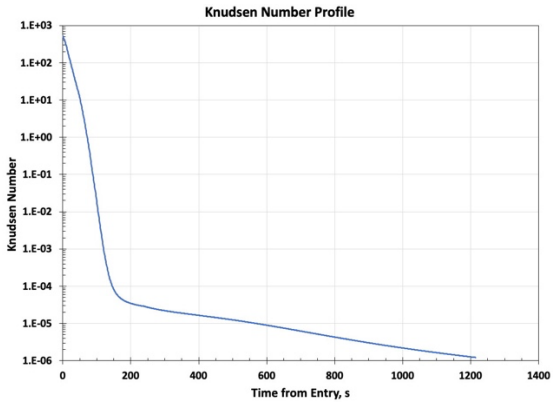

Figure 11 Nominal Knudsen number as a function of time from entry.

4.3 Pluto EAD Diameter Trade Study

In this mission study we performed a parameter study to determine the approximate maximum seam temperature Figure 12, internal gas pressure (Figure 13), and hoop stress (Figure 14) as a

function of EAD mass and diameter. These are the results from 675 entry trajectory runs, as will be described below.

To calculate the hoop stress, we used the formula: stress = pressure*radius/(2*thickness). We assumed a thickness of 0.07 mm for all EAD diameters. Note, the thermal model assumes a fixed 20 kg gas mass and a 70m diameter envelope. However, we adjusted the model and found that the results are nearly identical (within 2%) when the diameter and gas mass are adjusted in sync. This means that the results of this study are representative. Next, the thermal model assumes an areal density of the EAD to be 0.011 kg/m^2. We also adjusted this number and found that the maximum seam temperature changed by 4°C when we multiplied this areal density by 4. The internal gas pressure was unaffected. So, we believe the temperatures and internal pressures are within an error bound of a few percent of the reported results.

From the figures, the trend we see is that, above a certain mass, the maximum hoop stress and EAD temperatures are more sensitive to changes in EAD diameter than mass. If we choose to keep a 70 m EAD, we could go up to an entry mass of 1300 kg and still be below 700°C. Reducing the diameter of the EAD reduces the maximum hoop stress, but it also increases the EAD seam temperature. There is likely an optimal EAD diameter that balances maximum seam temperature and hoop stress that depends on the ultimate material properties of the EAD.

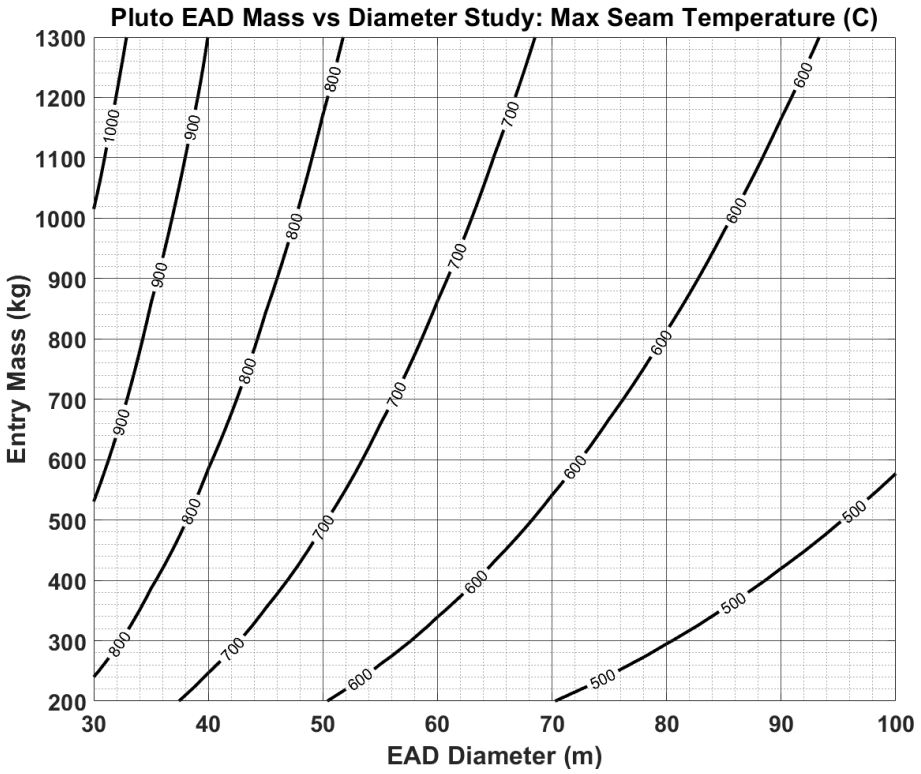

Figure 12 Mass vs. Diameter Study: Maximum seam temperature.

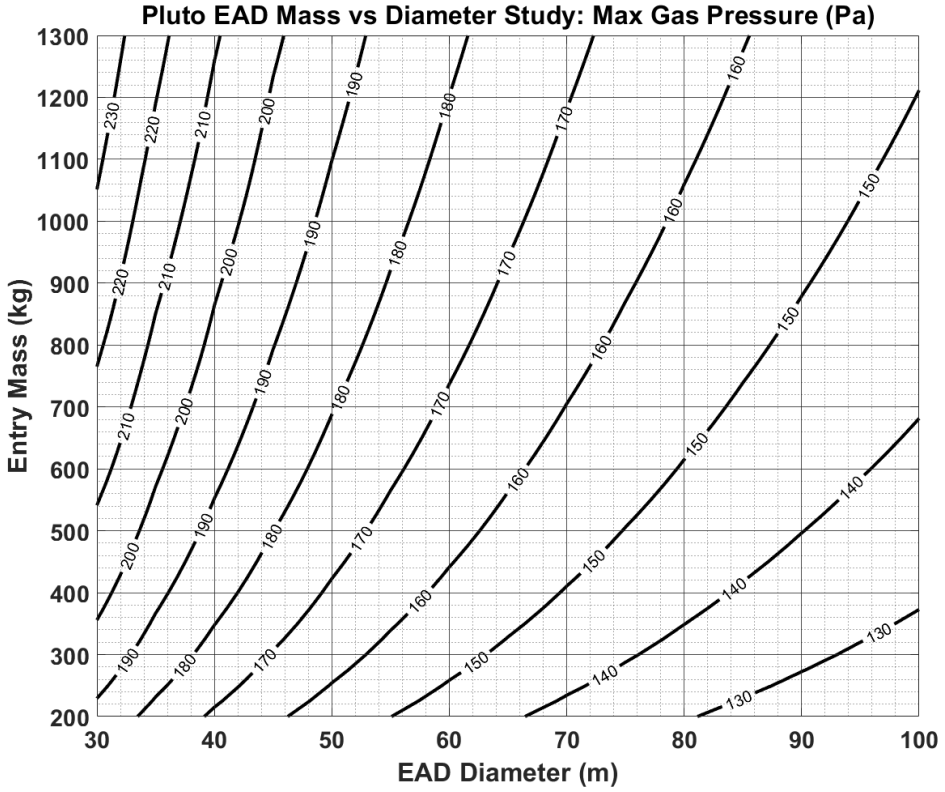

Figure 13 Mass vs. Diameter Study: Maximum gas pressure.

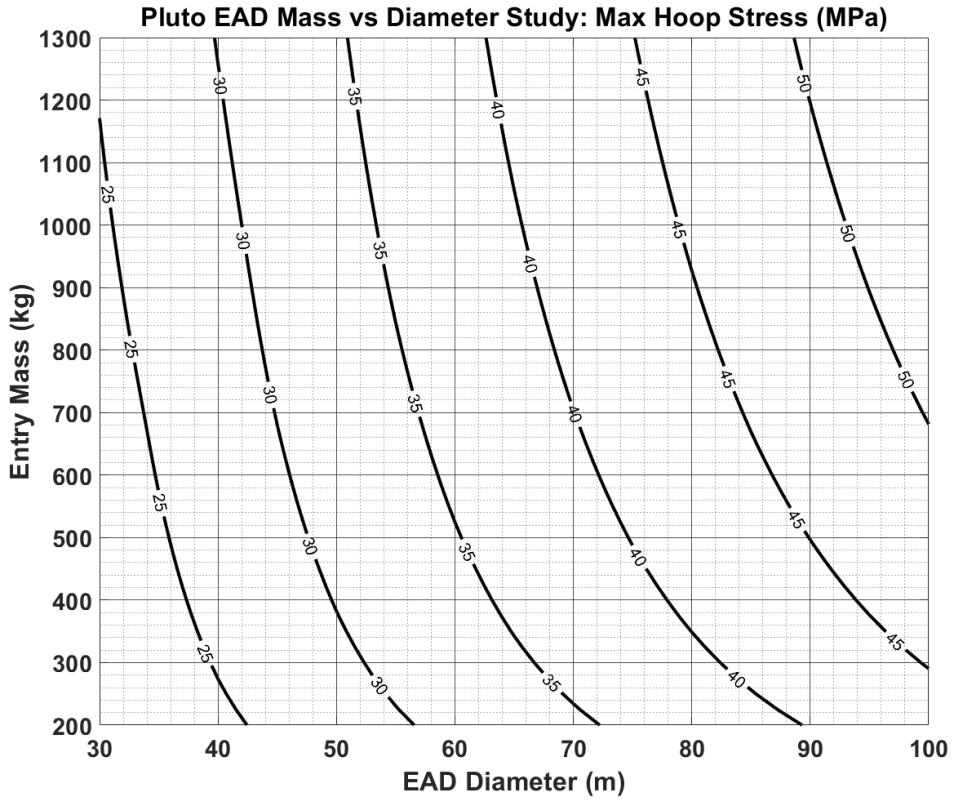

Figure 14 Mass vs. Diameter Study: Maximum hoop stress.

4.4 Pluto Landing Site Dispersion Analysis

A Monte Carlo analysis was performed to determine the Pluto landing site uncertainty given the expected trajectory, system, and atmospheric uncertainties. Monte Carlo simulations are utilized in engineering projects to map the effects of uncertainties in initial conditions on the results of a phenomenon of interest. In this specific example, uncertainties in the lander approach, spacecraft mass, cross sectional area, drag coefficient and planet atmosphere are mapped to a landing zone on the surface of Pluto along with their corresponding landing max heating rates, max dynamic pressures, and max accelerations during entry.

The Monte Carlo analysis was accomplished using a three degree of freedom entry analysis tool, HyperPASS, to map the contributions of key uncertainties in the approach trajectory and spacecraft properties to a landing zone area uncertainty. HyperPASS allows for the variation of aerodynamic properties with Knudsen number to account for transitions between free-molecular and continuum flow regimes.

A reference trajectory was assumed similar to the interplanetary mission used by New Horizons (NH) with an additional trajectory correction maneuver (TCM) at 7-days prior to arrival. The final Body Plane (B-Plane[§]) error ellipsoid is a 23.9 km 1σ semimajor axis, 17.1 km 1σ semiminor axis with a 62.3 s 1σ time of flight uncertainty as interpolated from the NH orbit determination (OD) solution history. Additional expected uncertainties in the atmospheric density profile at arrival (±4%), the spacecraft entry mass (±1.3%), EAD drag coefficient (10%), and EAD cross-sectional area (±0.32% or 1% circumference) were considered in the Monte Carlo analysis. It was found that the B-Plane uncertainties played the largest role in determining the size of the landing error ellipse. It may be possible to reduce the landing error ellipse with a TCM closer to arrival and/or with improvements to Pluto's ephemeris. The current estimated 3σ landing error ellipse is about 400 km by 190 km.

A nominal entry trajectory was selected based on several factors. The primary consideration is the entry flight path angle; aiming too steep risks extensive heating rates that could damage the lander and aiming too shallow risks large landing site errors or skipping out on Pluto's atmosphere. Figure 15 displays various trajectory parameters vs. time after entry for the nominal trajectory from the atmospheric interface at 1600 km altitude to Pluto's surface, flight path angle (FPA) of -63.4° with respect to the surface normal, for a landing aimpoint at 35.4ºW, 32.0ºN. The calculated nominal maximum stagnation heating rate was 3.65 W/cm^2, max dynamic pressure was 51.1 N/m^2, and the maximum acceleration was 28.8 gees.

Monte Carlo analysis is only as accurate as the assumptions made in determining the uncertainty variables. Table 2 gives a summary of the variables and assumptions made to create our Monte Carlo simulation. The distribution for all variations was assumed to be Gaussian.

[§] A plane normal to the incoming asymptote of the hyperbolic orbit that contains the target body's center of mass or, equivalently, normal to the velocity vector at "infinity" where infinity is defined to be far enough away from the periapsis of the hyperbola, such that the trajectory essentially lies on the asymptote. A B-vector is defined to be the from the target body's center of mass to that point where the V-infinity vector intersects the B-plane.

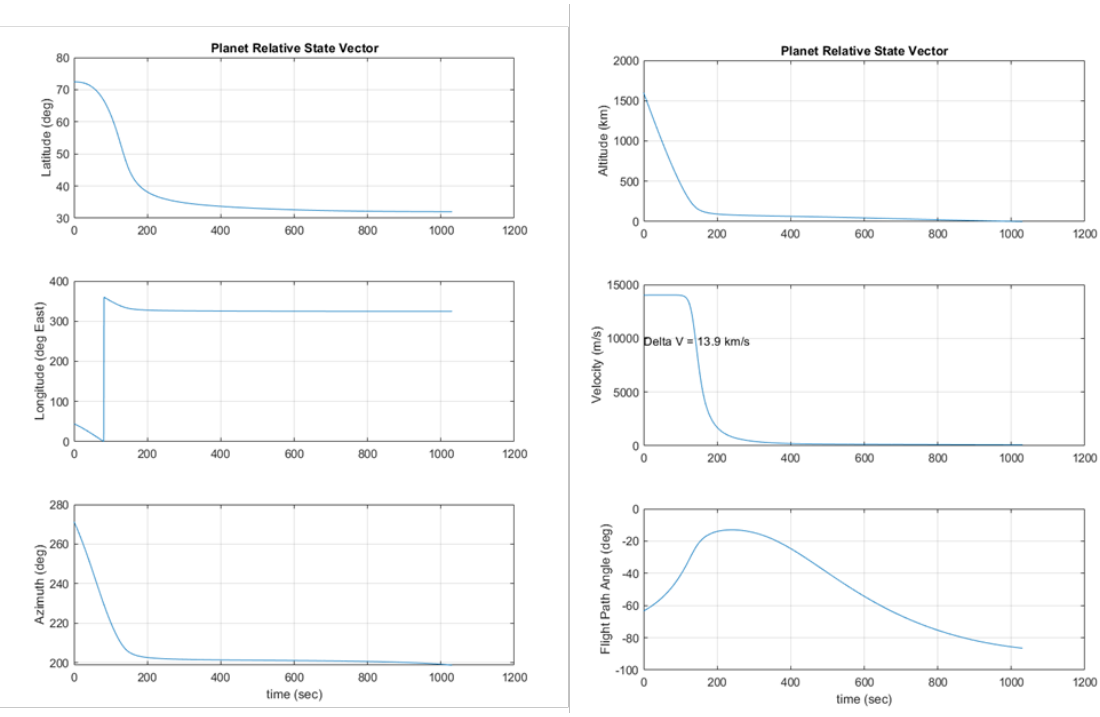

Figure 15 Nominal Trajectory Parameters as a Function of Time after Entry

Table 2. Monte Carlo Assumptions on Variables and their 1σ Uncertainties

Variable	1σ Uncertainties
Semi-Major B-Plane Ellipse, km	23.9
Semi-Minor B-Plane Ellipse, km	17.1
B-Plane Time of Flight, s	± 62.3
Atmospheric Density Profile	± 4.04%
Hypersonic Drag Coefficient	± 3.33%
Entry Mass, kg	± 2.2
Envelope Cross-section Area, m^2	± 25.73

4.4.1. B-plane Target Error Ellipse

One of the largest contributors to the uncertainty is the B-plane targeting error ellipse. The size and orientation of the 1σ B-plane uncertainty ellipse are derived from the evolution of the NH approach uncertainty ellipse. It was determined that an additional trajectory correction maneuver (TCM) at 7 days to periapsis (T-7) would be required for an acceptable landing error ellipse.

Figure 16 displays the NH OD solutions as plus marks [+] in a semi-major and semi-minor error ellipse axis as a function of time out to encounter minus 50 days. Optical navigation was begun about 100 days prior to encounter. To estimate the fit at different times, we generated a quadratic fit of the semi-major and semi-minor axis of the 1σ B-plane error ellipse using the NH OD solution points that are shown as the blue curve in the semi-major axis chart and as a red curve in the semi-minor axis chart. A 2^{nd} order model chosen over 3^{rd} and 4^{th} orders because it gave the best compromise between accurately fitting the data and artificially tracking data points. For example, a 3^{rd} order model predicted a smaller major and minor axis ellipse error than the Crit 32 solution, which was deemed not realistic in our judgement.

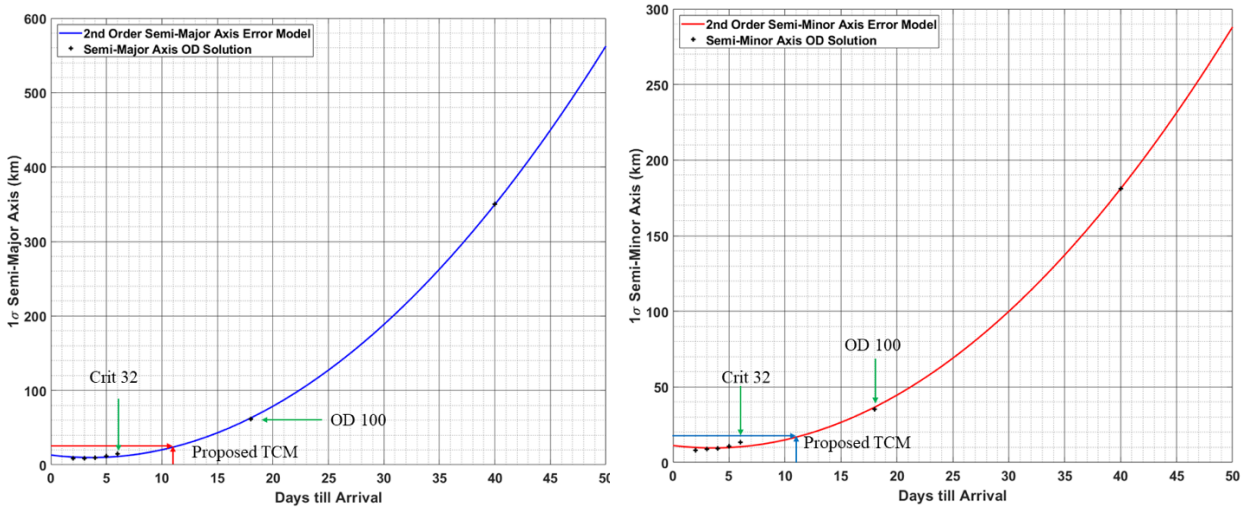

Figure 16 New Horizons B-plane 1σ semi-major and semi-minor error ellipse fit.

We also assumed a four-day buffer was needed between the OD solution and a TCM to allow for planning, data processing, and the 9-hour time delay to send signals between the spacecraft and Earth. Hence a 7-day TCM relied on an OD from periapsis minus 11 days (T-11). The 1σ time of flight error is found by a linear interpolation of the NH OD100 and Crit32 solutions time of flight error. These initial OD errors are shown in Figure 17 that zooms in to the final 20 days before encounter. Additional errors are added to the error ellipse to account for uncertainties in the final TCM. The procedure to find the final 1σ TCM error is as follows: first assume the same ΔV error as the final New Horizon TCM-17B1. Then assume a worst case that the ΔV uncertainty is entirely within the B-plane. Multiply the ΔV uncertainty by the time to arrival to get the effect of the final TCM error on the total B-plane ellipse. The final B-plane error ellipse is found by root sum square of the TCM error and the OD solution fit. The final values are reported in Table 2.

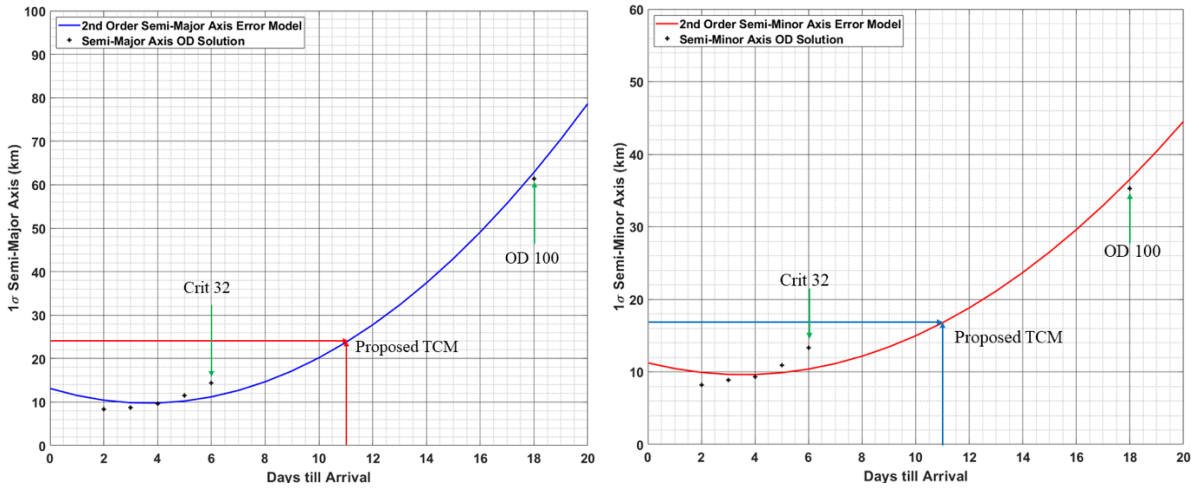

Figure 17 New Horizons B-plane 1σ semi major and minor error ellipse fit zoomed in to the last 20 days showing the errors for T-11 days that were used as initial conditions in the Monte Carlo analysis.

4.4.2. Atmosphere Uncertainty

In 2015, the NH mission flew by Pluto and measured the condition of its atmosphere. One surprising result was that its atmosphere probably never totally condenses out into ice as it moves toward aphelion, i.e., there is always some atmosphere, but it varies. Developing an accurate model of the density and temperature profile of Pluto is an important criterion for determining the landing error ellipse of the lander. Pluto's average surface pressure and density profile depend on heliocentric distance and the location of the subsolar point. Reservoirs of mostly frozen surface nitrogen and other compounds freeze and thaw throughout the 248-year orbital period changing the dynamics of the atmosphere. Recent star occultations and NH results of the surface nitrogen reservoirs have updated Pluto's surface pressure evolution models as presented by Meza**.

Pluto's atmospheric density has been modeled in Meza based on star occultations and the expected vaporization and condensing of the atmosphere assuming different nitrogen ice albedos. The evolution of the atmosphere as a function of solar longitude of Pluto is shown in Figure 18. This figure displays a typical modeled annual evolution of surface pressure obtained with *Laboratoire de Météorologie Dynamique* Pluto volatile transport model††, assuming permanent deposits of N_2 ice, a uniform soil seasonal thermal inertia, an emissivity $\varepsilon_{N2} = 0.8$ and albedo range $A_{N2} = 0.72$–0.73 for N_2 ice, chosen to yield a surface pressure near 10–11 µbar in July 2015 near the New Horizons flyby date. The black dots with error bars show the surface pressure (p_{surf}) inferred from stellar occultation measurements. The curve in magenta corresponds to a similar simulation but assuming a permanent N_2 ice reservoir in the south hemisphere between 52.5°S and 67.5°S, which leads to a pressure peak in 1990.

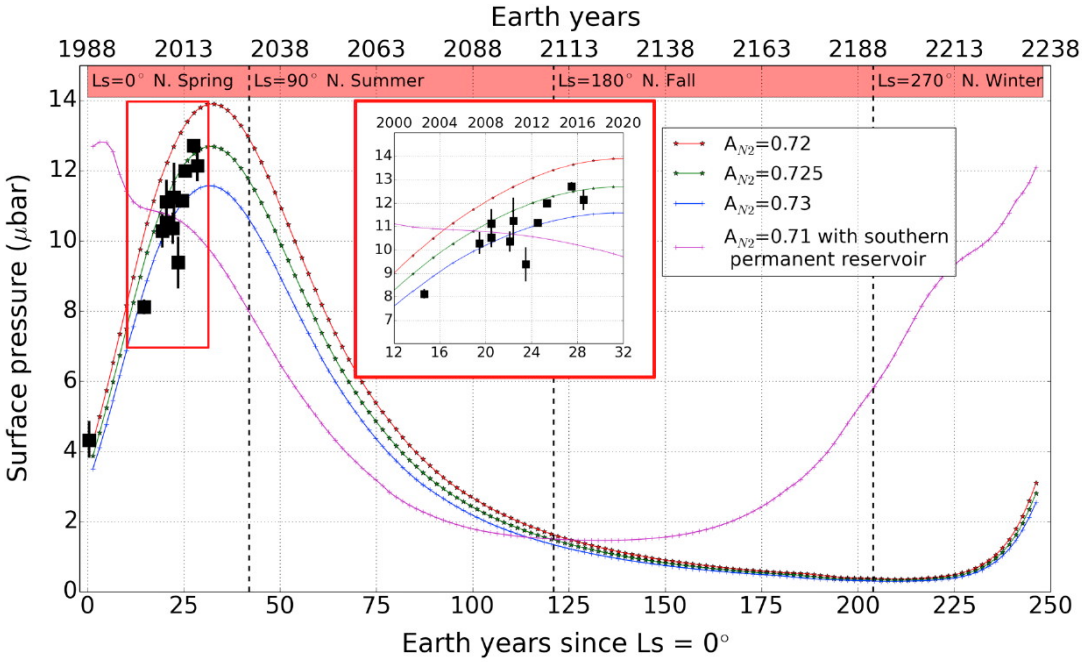

Figure 18 Evolution of Pluto's atmosphere

** Meza, E., et al. (2019). Lower atmosphere and pressure evolution on Pluto from ground-based stellar occultations, 1988–2016. *Astronomy & Astrophysics, 625*. https://doi.org/10.1051/0004-6361/201834281

†† Designed to simulate the volatile cycles over seasonal and astronomical timescales on the whole planetary sphere.

We took the density and temperature atmospheric profile given by Strobel[‡‡], and assumed a constant ratio between the density profile during the New Horizons flyby (ρ_{NH}) and the expected arrival time (ρ_a). Assuming an ideal gas, ($P = \rho R_g T$) where P, ρ, R_g, and T are gas pressure, density, specific gas constant and temperature respectively, and that Pluto's average surface temperate is constant year-round Meza we get that the scaling factor (q) is equal to the ratio between Pluto's surface pressure at arrival and the New Horizons flyby (P_{NH} & P_a).

Assuming permanent nitrogen deposits and an albedo of $A_{N2} = 0.725$, the model in Meza, predicts q will be roughly 0.74 during the time of arrival. Knowing this, we constructed a nominal atmospheric density profile and present it in Figure 19.

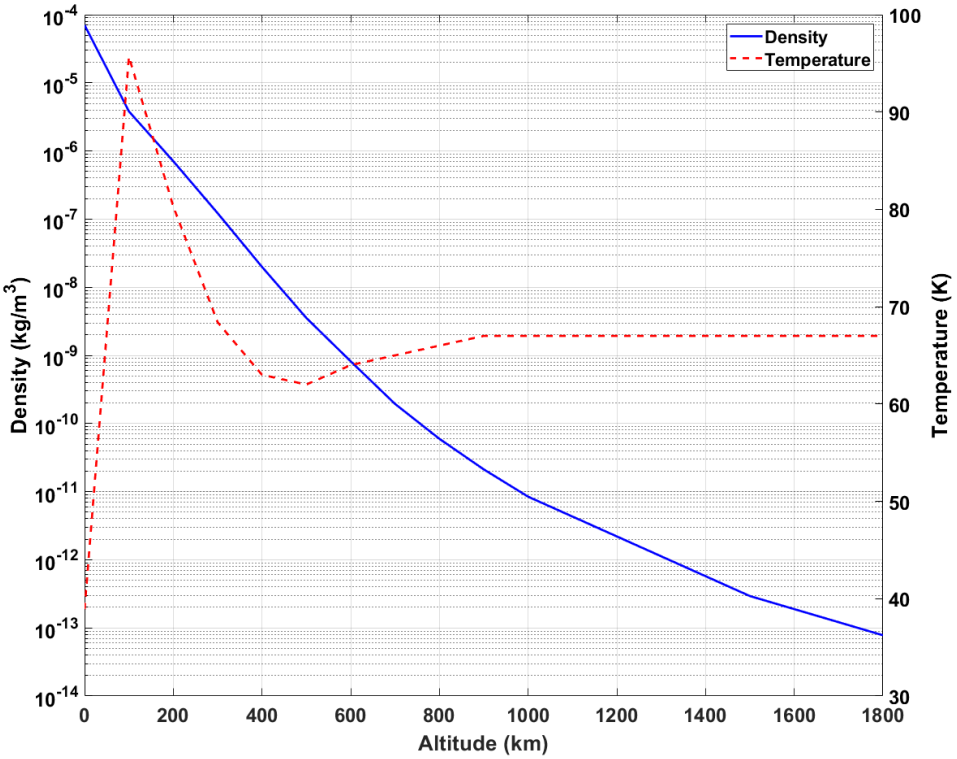

Figure 19 Expected Pluto atmosphere at arrival.

We assumed that data from a star occultation will be available close to the lander's arrival window; the spacecraft will be able to make the necessary maneuvers in case the measured density profile is different from the current best estimate. Therefore, the uncertainty in q lies in the star occultation measurement. We averaged the surface pressure error estimates reported by Meza and assumed the error in P to be normally distributed with a standard deviation equal to this average error. We calculate the standard deviation of q to be about 0.04 from the estimated error in P by implementing the statistical analysis for division error. In summary, our Monte Carlo simulation used an atmosphere density profile of New Horizons scaled according to a normal distribution with a mean of 0.74 and a standard deviation of about 0.04.

[‡‡] Strobel, D. F., & Zhu, X. (2017). Comparative planetary nitrogen atmospheres: Density and thermal structures of Pluto and Triton. Icarus, 291, 55–64. https://doi.org/10.1016/j.icarus.2017.03.013

4.4.3. Drag Coefficient

Our aerodynamic entry model varies the vehicle drag coefficient with the Knudsen and Mach numbers based on a spherical geometry. During entry the spacecraft moves through three different flow field regimes: free-molecular, transitional region, and finally continuum. Figure 20 displays the EAD drag coefficient as a function of altitude with the flow field regimes illustrated. Figure 21 displays this same data, but as a function of time.

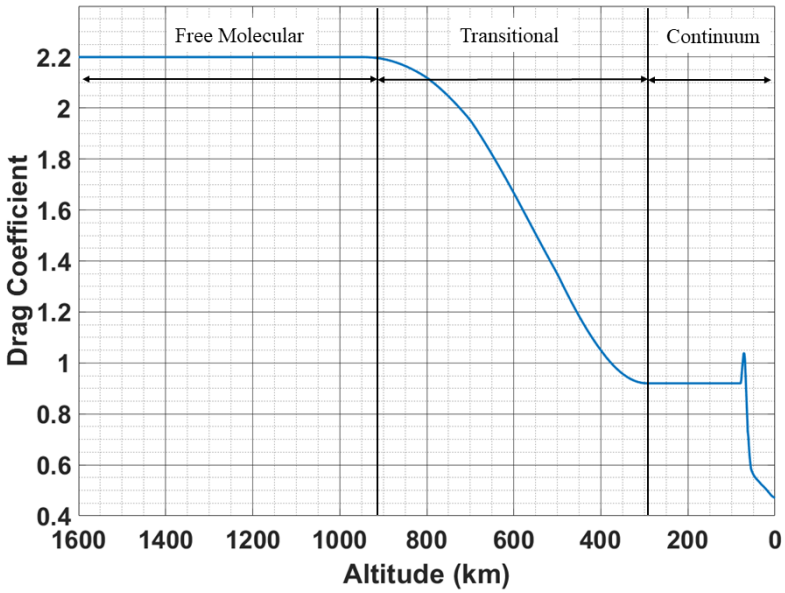

Figure 20 EAD drag coefficient as a function of altitude during entry.

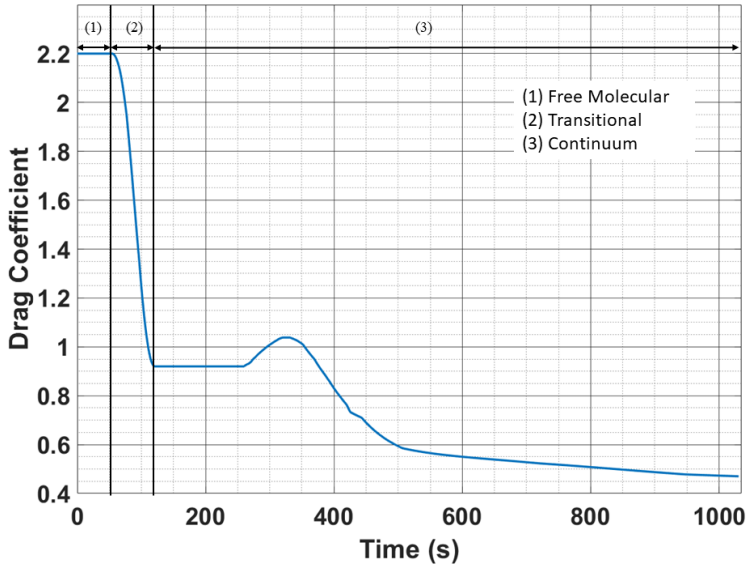

Figure 21 EAD drag coefficient as a function of time during entry flow regions (1) free-molecular, (2) transitional region, and (3) continuum.

Knudsen number is defined as the mean free path divided by the size of the object. The free molecular region is defined when the Knudsen number is greater than 10. In this region, the mean

free path of a particle is greater than the relevant characteristic length or, in this case, the diameter of the EAD. Our early analysis showed that variations as high as ±10% in the free molecular drag coefficient had negligible effects on the landing zone uncertainty and trajectory characteristics. This is because the atmospheric density in this region is almost zero and, as shown in Figure 21, the spacecraft trajectory spends little time in the free molecular region after entry, leading to an inconsequential total drag. For this reason, we chose not to vary the free molecular region drag coefficient in the Monte Carlo analysis, and instead assigned a constant value of 2.2 based on Baker[§§].

The transitional region is defined by Knudsen numbers between the free molecular and continuum critical values. The drag coefficient in this region is determined by using a fitting function of Knudsen number to create a smooth transition between the free molecular drag coefficient and the hypersonic continuum drag coefficient.

The continuum region is defined as the parts of the trajectory with Knudsen numbers less than 0.001. The drag coefficient is a function of the Mach number and the Reynolds number. However, at supersonic and hypersonic speeds the Mach number becomes the dominate determining factor for the drag coefficient[***]. For this reason, the drag coefficient is computed by a data table look up from Carter[†††] using the estimated Mach number calculated at each time step. Early analysis showed that small variations in this region's drag coefficient had the greatest impact on the landing zone uncertainty. Following a similar process to Desai[‡‡‡], we chose to shift the drag coefficient data table by ± 10% the nominal value to account for the drag coefficient uncertainties. We assume the shift factor has a normal distribution with a mean of 0% and a standard deviation of 3.33%.

4.4.4. Entry Mass and Cross-section Area

The other key components of the entry system ballistic coefficient are entry mass and cross-section area. Three distinct mass uncertainties are considered in the Monte Carlo analysis. First is the uncertainty in the total amount of propellant used for TCMs and attitude control during the interplanetary cruise since the spacecraft can make proper ephemeris changes with total mass updates. We found the uncertainty percentage of used propellant for the New Horizons spacecraft at the time of the Pluto flyby[§§§] and applied the same percentage to our fuel propellant systems assuming we use 100% of the propellant fuel available. Next, we assume a standard 2% mass uncertainty in the inflation gas and a 1% mass uncertainty in the total MEV mass in the spacecraft due to weighing uncertainty. After taking the rms of these values we obtain the final 1σ mass uncertainty of 2.179 kg.

For the EAD cross-sectional area uncertainty, we assume the final measurement of the EAD circumference after construction would be the major source of uncertainty. We assume a 3σ 1% uncertainty circumference measurement leading to a normal EAD radius distribution with a mean of 35 m and a standard deviation of 0.117 m, which corresponds to a 1σ cross-section area error of ± 25.78 m^2 or about ±0.7%.

[§§] Baker, R. (1967). Astrodynamics. Applications and Advanced Topics.

[***] Gerhart, P. M. (2018). Fundamentals of Fluid Mechanics, 8th edition. Wiley.

[†††] Carter, Robert T. et al. "Estimating the Drag Coefficients of Meteorites for all Mach Number Regimes." (2009).

[‡‡‡] Desai, P., R. Mitcheltree, and F. Cheatwood. (1999). Entry Trajectory Issues for the Stardust Sample Return Capsule.

[§§§] Bushman, S. S. (2017). Performance of the new horizons propulsion system through the Pluto Encounter. 53rd AIAA/SAE/ASEE Joint Propulsion Conference. https://doi.org/10.2514/6.2017-4746

4.4.5. Monte Carlo Analysis Results

Figure 22 presents the results of the Monte Carlo simulation with 10,000 individual cases for an aim point at 35.4°W, 32.0°N on the surface of Pluto. Additionally, three curves of selected constant flight path angles are plotted that map out different longitude/latitude aim points. These lines represent the different landing sites predicted when varying the B-Plane entry point while keeping a given flight path angle. By adjusting the time of arrival and including the hopping range any latitudes touched by these curves are available for landing. The lander can land anywhere between the FPA of -62° and -65° curves by altering its B-Plane position. Aiming below this range risks the spacecraft burning up on reentry, while aiming too high risks the spacecraft skipping out of the atmosphere or landing on dark side of the planet where it cannot communicate with Earth.

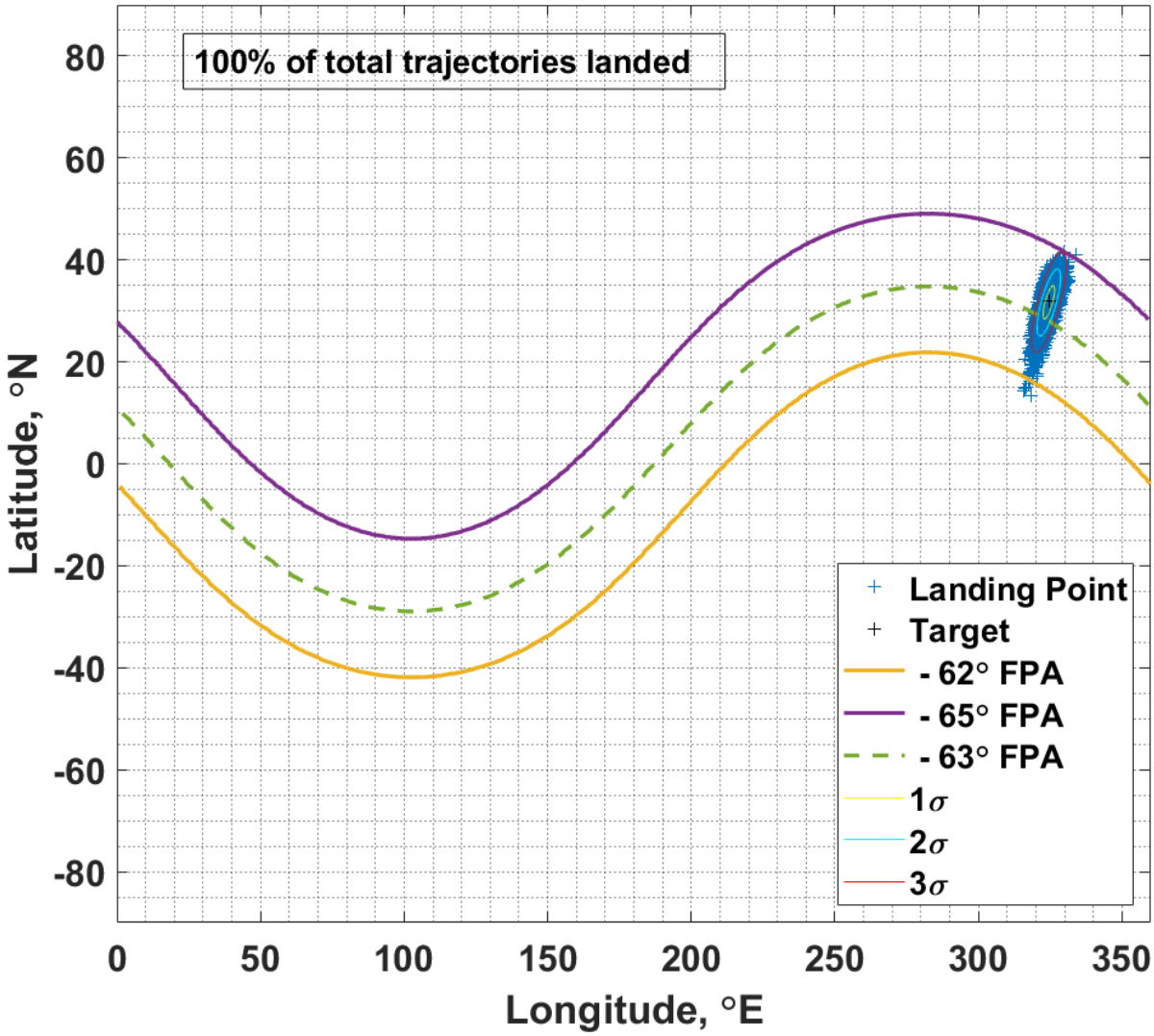

Figure 22 Landing error ellipse for a 35.4°W, 32.0°N aimpoint

Figure 23 is a closeup of the landing zone showing the FPA and one, two and three sigma landing error ellipses.

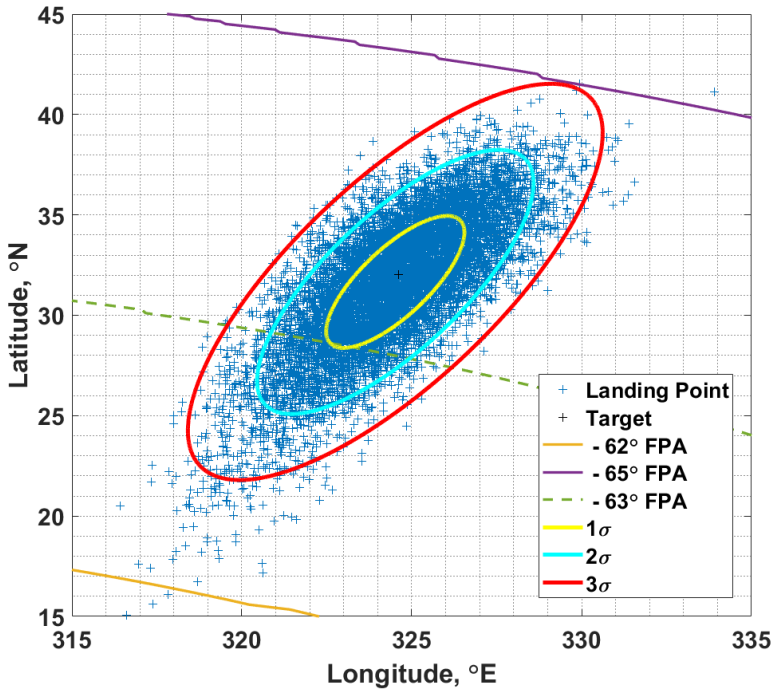

Figure 23 Detail of landing error ellipse for a 35.4°W, 32.0°N aimpoint

Figure 24 illustrates the possible latitudes and surface features for landing assuming a varying arrival time and combining both the target flight path angle limitation and desire for having some view of the Earth after landing for communications.

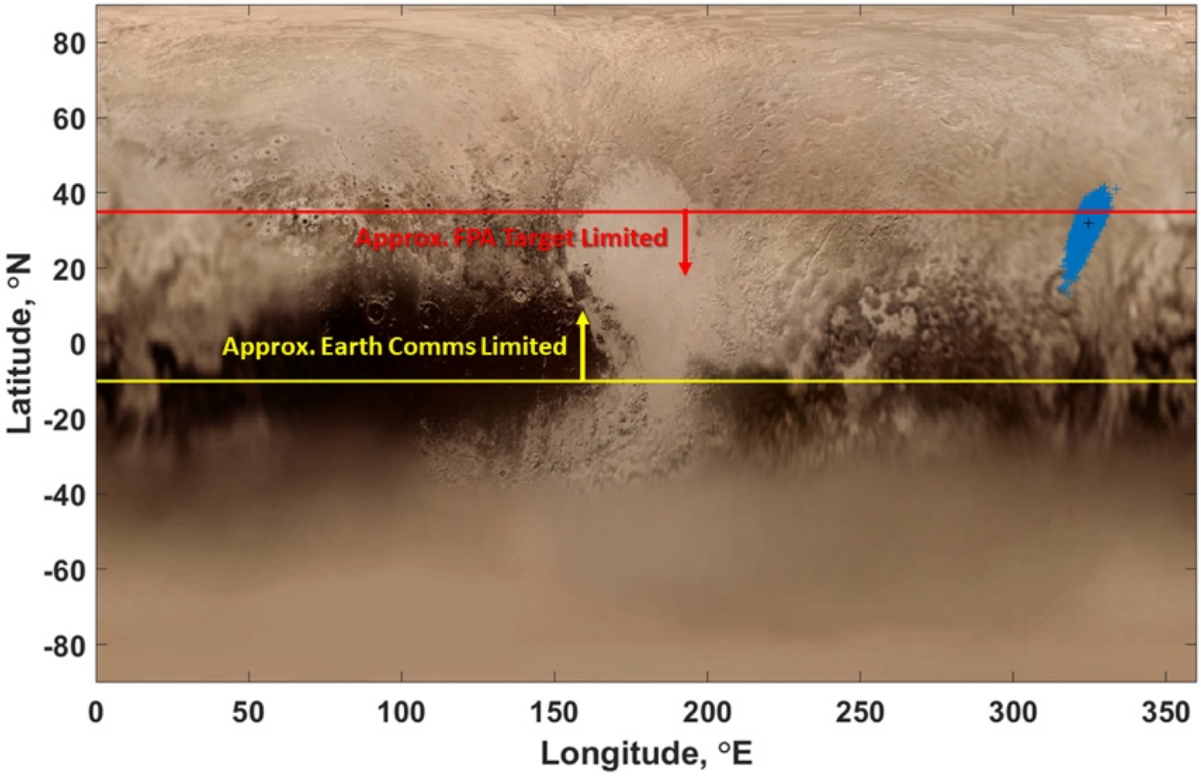

Figure 24 Possible Landing Latitudes

The further north the landing site, the longer the Earth communications periods. The target flight path latitude limit was chosen roughly as the tip latitude of the -63º FPA curve because any point on Pluto's surface with a latitude reached by the -63º FPA curve can be reached with a combination of varying the B-plane target and arrival time. The FPA target latitude was calculated to be roughly 35ºN and represents a rough safe target limit. In fact, the simulation shown in Figure 22 and Figure 23 have a target aimpoint with a -63.4º entry FPA, but the -63º FPA curve was chosen for FPA target latitude limit for a higher margin of safety. In Figure 22 and Figure 23, the 3σ landing error ellipse is below the -65º FPA curve and only the extrema have entry FPAs near -65º. This means that the FPA target latitude shown in Figure 24 represents a maximum latitude for the nominal aimpoint of a Pluto mission using an EAD around the current target arrival time. As shown in Figure 24, some trajectories can land with latitudes above this flight path target limit line, but a target/aimpoint with a greater latitude than the FPA target limit line has substantial probability of having an entry flight path angle beyond the -65º FPA limit and can potentially overheat.

4.5 Application of EAD Technology to Other Missions

In this section we discuss the application of EAD to missions beyond a Pluto Lander. These mission applications currently include a similar mission to Neptune's largest moon, Triton; a space station crew or passenger rescue pod; and a neutral atmospheric density monitoring system.

4.5.1. Assessment of EAD Application for Outer Planet Satellite Atmospheres

We conducted a study of other solar system bodies with tenuous atmosphere besides Pluto and Triton, to see if there were any other targets that might be favorable for using EAD for entry and landing.

In the Jupiter system we examined Ganymede, Callisto, Io and Europa. Ganymede is the largest Solar System body without a substantial atmosphere. Its surface pressure is about 3 orders of magnitude lower than atmosphere of Pluto and Triton. Callisto is surrounded by an extremely thin atmosphere composed mostly of O_2, however its surface pressure is less than Ganymede. On Io's dayside, the atmosphere density peaks, however even there it is 5-6 orders of magnitude lower than Pluto. The atmosphere of Europa can be categorized as thin and tenuous (often called an exosphere), primarily composed of oxygen and trace amounts of water vapor. Surface pressure is about 4 orders of magnitude lower than the atmosphere of Pluto or Triton.

In the Saturn system we examined Enceladus and Rhea. At Enceladus, a trace atmosphere has been observed with significant spatial variability. The James Webb Space Telescope recently saw a surprisingly large, 10,000 km plume jetting from its surface. Cassini observed an atmosphere from magnetometer measurements. Its UV Imaging Spectrometer observed two star occultations, and discovered the atmospheric molecules are likely water, and column densities have been estimated. The combined analysis of imaging, mass spectrometry, and magnetospheric data suggests that the observed south polar plume emanates from pressurized subsurface chambers, like Earth's geysers or fumaroles. The mechanism that drives and sustains the eruptions is thought to be tidal heating. The intensity of the eruption of the south polar jets varies significantly as a function of the position of Enceladus in its orbit. This is consistent with geophysical calculations which predict the south polar fissures are under compression near periapsis, pushing them shut, and under tension near apoapsis, pulling them open. At Enceladus, it appears that cryovolcanism occurs because water-filled cracks are periodically exposed to vacuum, the cracks being opened and closed by tidal stresses. If one could predict when a crack will open and release a water plume, the density could

be enough to slow an EAD sufficiently to land, however this timing would require extremely accurate navigation and plume eruption predictions, which are problematic. Rhea also has a tenuous atmosphere; however, its surface density is roughly equivalent to Earth density at 900 km altitude, which is not enough to do any significant deceleration with EAD.

In the Uranus system, only Titania may offer a tenuous atmosphere, however, an upper limit of its surface pressure is about 6 orders of magnitude lower than Pluto or Triton.

Hence, the only bodies in the solar system with enough tenuous atmosphere to enable using an EAD for entry and landing are Pluto and Triton.

4.5.2. Triton Lander Mission Analysis

Two Triton lander mission modes are envisioned, namely, direct entry of a large lander from a hyperbolic trajectory and entry and landing from a Neptune orbiter. The former mission mode involves similar sized EAD systems to the Pluto lander. The latter mission mode enables a small, short duration lander deployed as a secondary payload from a Neptune orbiter, which could be a flagship-class mission.

In the Neptune orbiter secondary payload mode, the relevant Triton mission and system parameters are shown in Table 3. These data assume the orbiter is in a 20-day period orbit of Neptune, the mass of the lander EDL system on board the orbiter is 48 kg, the EAD diameter is 14 m, and the non-propulsive mass delivered to the surface of Triton is 20 kg including science instruments. For this analysis, we have assumed the Triton surface atmospheric pressure is about 1.4 Pa.

Table 3. Small Triton Lander Mission and System Parameters

Entry, Descent and Landing Parameters	Triton Lander Values
Orbiter Period, days	20
On-orbit / Entry Mass, kg	48 / 34
Entry Speed, km/s	4.3
Envelope Diameter, m	14
Peak Heating Rate, W/cm^2	0.8
Peak g-load, gees	23
Peak Dynamic Pressure, Pa	52
Landing Delta-V, m/s	99
Landed / Non-propulsive Mass, kg	26 / 20

A direct entry Triton lander mode could be more challenging than a small lander deployed from a flagship-class Neptune mission since the Neptune V-infinity and Triton approach speeds can be much higher, plus Neptune's gravity will increase the entry speed of the lander beyond the Neptune V-infinity on the approach to Triton. In addition, such a lander would be expected to be similar in mass and capability to a proposed Pluto lander.

Given two recent proposed mission concepts to the Neptune-Triton system, the Neptune approach V-infinity velocities could be from about 10.7 km/s[****] to 20.9 km/s[††††]. Given this range of

[****] Landau, D. and N. Strange, Outer Planet Flagship Missions with ARM---derived Electric Propulsion Stage, Poster, NASA/JPL, March 6, 2015.

[††††] Howett, C., K. Mitchell, and L. Prockter, Trident – A mission to Triton, presentation, August 31, 2020.

Neptune approach velocities, and assuming a tangential and co-orbital Triton approach geometry, the Triton entry speeds could be between 8-18 km/s.

For the 8 km/s Triton entry speed and the same lander mass as for the Pluto lander, the EAD diameter is only 40 m. Entry heating is about 2 W/cm^2 and peak g-load is about 20 gees, both less than for Pluto, and the landing delta-V is 115 m/s.

For the 18 km/s case with an EAD diameter the same as for Pluto of 70 m and a smaller entry mass of 430 kg, the peak heating is almost double than for Pluto at 6.5 W/cm2 and peak g-load is higher at about 50 gees, which are more challenging than for a Pluto mission and results in a smaller, 130 kg lander. A 200 kg lander would require increased EAD diameter or increased heating and g-loads.

4.5.3. Application of EAD to Aerocapture at Neptune

In this section we discuss the application of EAD to Neptune aerocapture using the atmosphere of Triton. In this work we assumed a hyperbolic approach velocity (V-infinity) of 11 km/s, which is typical of a 11–12-year transit time to Neptune. We also assume that the encounter geometry is co-orbital and coplanar with Triton, which therefore assumes the lowest possible Triton entry speed. The mission parameters are presented in Table 4.

Table 4 Neptune Aerocapture using Triton's Atmosphere.

Mission Parameters	Values
Neptune V-infinity, km/s	11
Triton Approach Geometry	Coplanar/Co-orbit
Triton Entry Mass, kg	640
Neptune Orbiter Mass, kg	500
EAD Envelope Diameter, m	20
Minimum Triton Altitude, km	70
Neptune Orbiter Period, days	60

This analysis indicates that a 60-day period orbit could be achieved by a Triton aerocapture pass. Figure 25 through Figure 28 display some key parameters during the Triton aerocapture event.

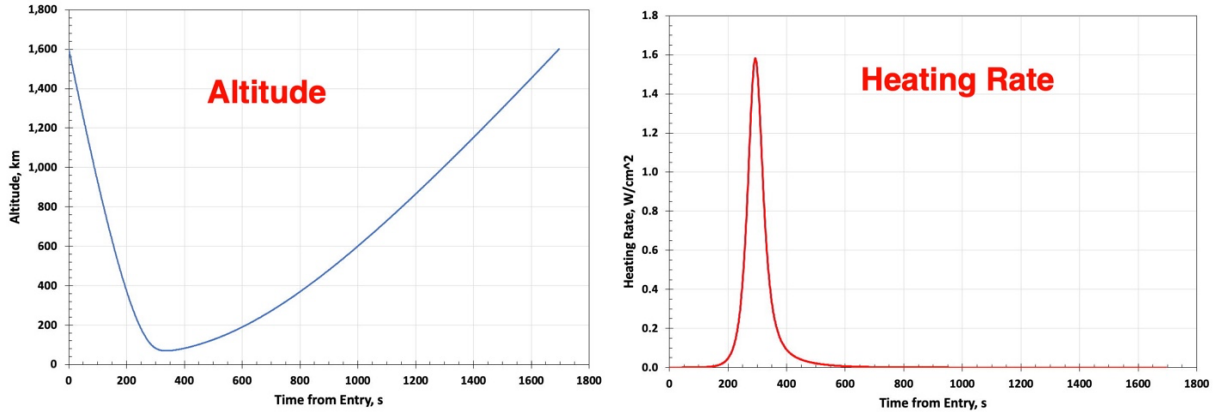

Figure 25 Altitude and Heating Rate vs. Time.

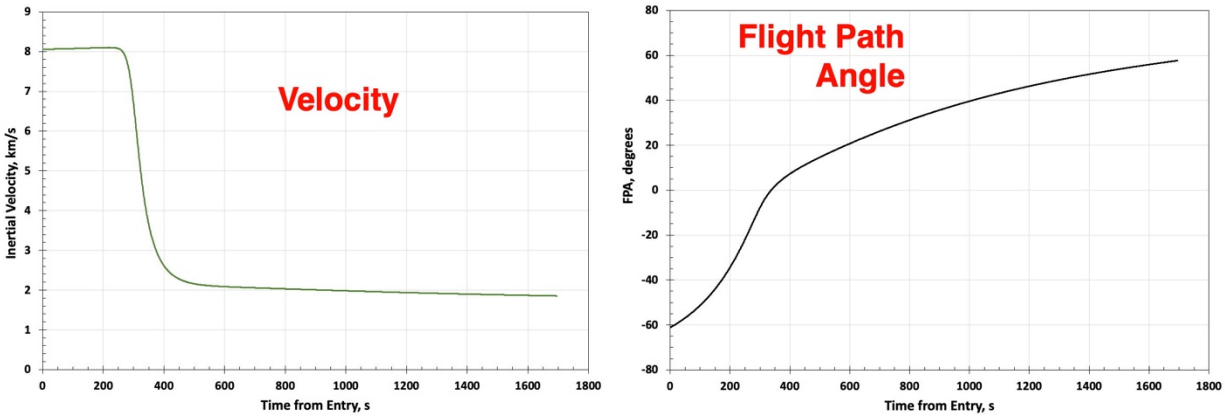

Figure 26 Velocity and Flight Path Angle vs. Time.

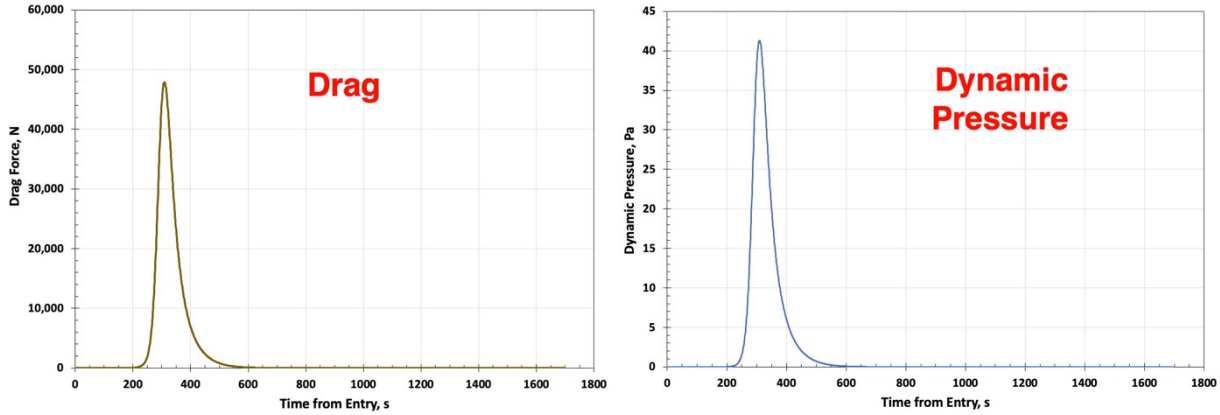

Figure 27 Drag and Dynamic Pressure vs. Time.

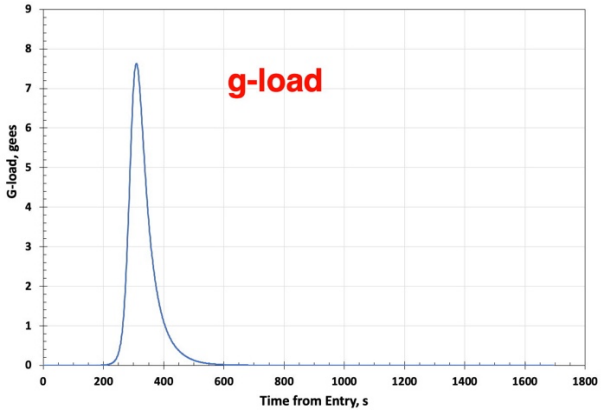

Figure 28 G-load vs. Time.

We compare these data with a direct aerocapture of Neptune‡‡‡‡ with same V-infinity and roughly the same entry system and the heating rate is about a factor of 5 higher than using Triton's atmosphere, which would exceed the peak temperature limit of the EAD.

‡‡‡‡ D. Lyons and W. Johnson, Ballute Aerocapture Trajectories at Neptune, AIAA/AAS Astrodynamics Specialist Conference and Exhibit, Providence, RI, 2004.

4.6 Eliminating Need for Jupiter Gravity Assists

The current reference trajectory for the Pluto lander mission includes a gravity assist of Jupiter in order to keep the flight duration shorter than about 11 years. But it is clear that a Pluto mission launching that soon is not currently feasible. Therefore, a similar mission would have to slip to the next Jupiter gravity assist window 12-13 years later.

An alternate interplanetary trajectory mode is to consider using Solar Electric Propulsion (SEP) combined with multiple Earth-Venus gravity assists. This mission mode is not new, however its application for a New Frontiers-class mission may be. The advantages of this mission mode are the following:

- Does not rely on periodic Jupiter alignment
- Likely available frequently to Outer Planets targets
- Takes advantage of the Sun's gravity well for doing propulsive and gravity assist maneuvers
- Benefits from increase solar radiation inside 1 AU, e.g., double the solar array power at Venus orbit radius
- Does not require radiation hardening of electronics
- The value of this mission mode is a good fraction of the cost of a very large launch

We obtained the NASA/JPL Mission-Analysis Low-Thrust Optimization (MALTO), to conduct a very preliminary analysis of the trajectory possibilities. The parameters we analyzed we as follows:

- Launch Mass: 1600-2400 kg
- Launch Vehicle: Falcon Heavy
- Xenon Propellant Mass: 400-1000 kg
- Solar Electric Propulsion (SEP) Mass: 300-600 kg
- SEP System
    - 3 or 4 NEXT-C Thrusters (Isp ~4200s)
    - 7.5 or 15 kW Ultraflex Solar Array

Note the thruster and solar array have spaceflight heritage.

Very preliminary results are shown in Figure 29 and Figure 30. Figure 29 displays a 15-year flight to Pluto requiring an Earth-Venus-Earth-Earth-Pluto (EVEEP) trajectory sequence. Key parameters for this opportunity are launch mass of 2433 kg, arrival mass of 1950 kg, including the SEP stage, and an arrival V-infinity of 13.2 km/s. Figure 30 displays a 12-year flight to Pluto requiring an Earth-Venus-Earth-Neptune (EVEN) trajectory sequence. Key parameters for this opportunity are launch mass of 1545 kg, arrival mass of 1003 kg, including the SEP stage, and an arrival V-infinity of 10.4 km/s.

These trajectories are not optimal having arrival masses too low or flight times longer than desired, however they suggest what might be possible with further study.

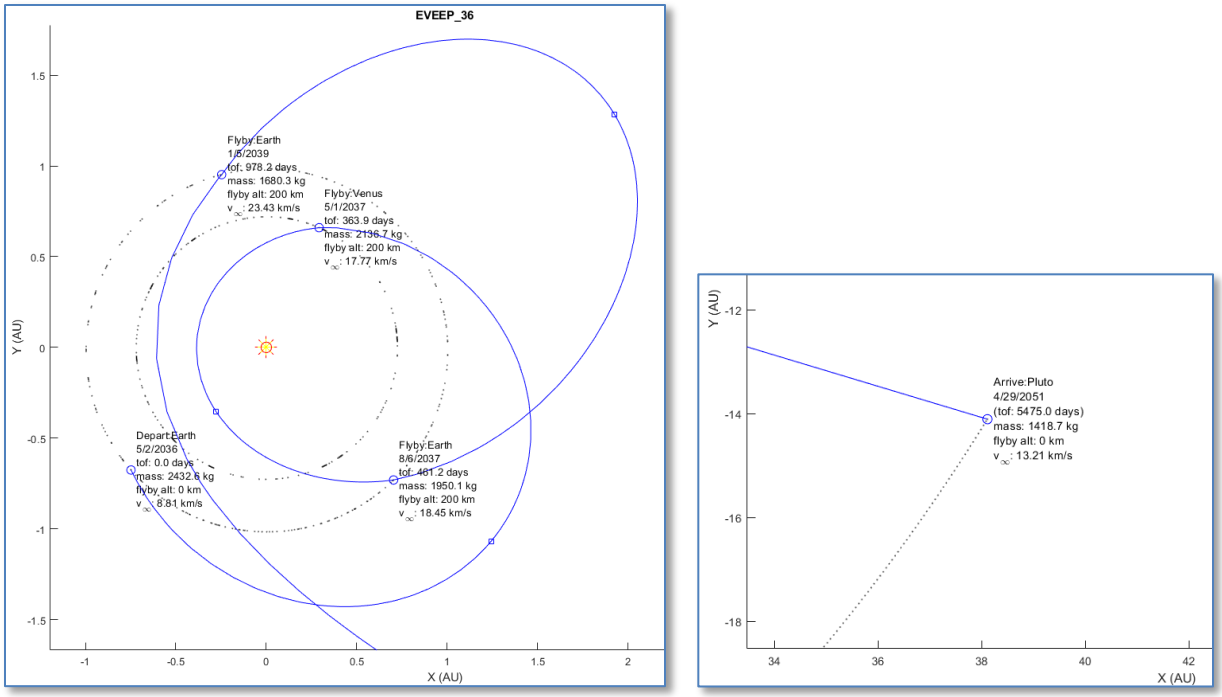

Figure 29 EVEEP trajectory to Pluto

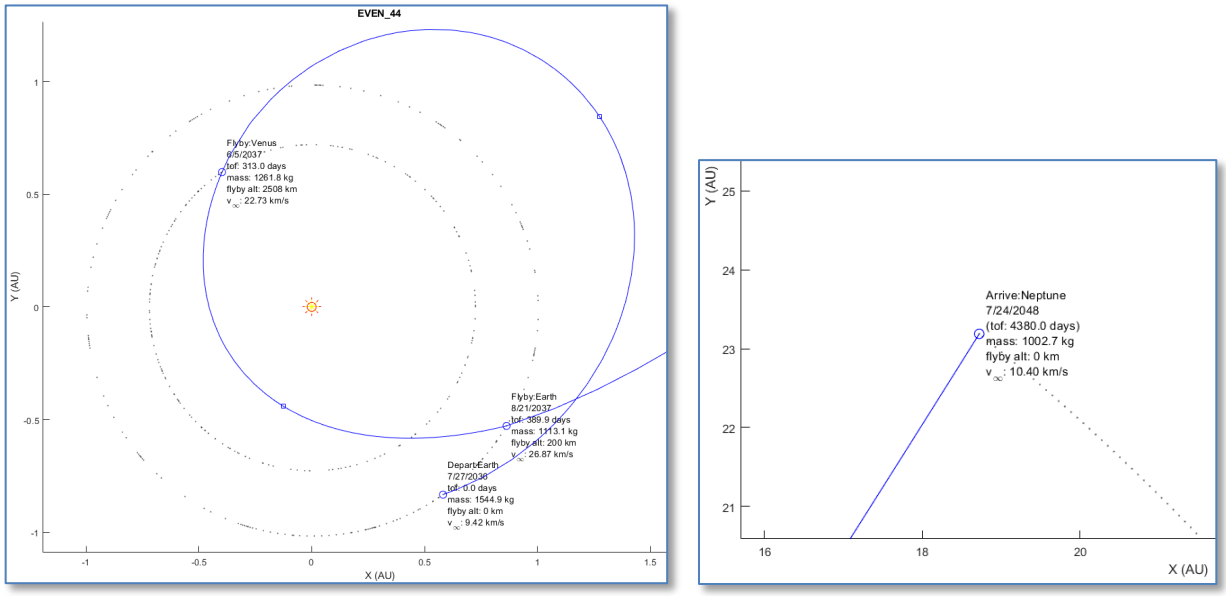

Figure 30 EVEN trajectory to Neptune

4.7 Technology Spin-offs

During the Phase II effort we developed two spin-offs of the EAD technology, namely a ***Space Station Escape Pod*** and a ***Neutral Atmospheric Density Monitoring System***, which are discussed in the next two sections.

4.7.1. Space Station Escape Pod

A space station Rescue Pod offers an independent space station rescue capability. A Rescue Pod is an inflatable reentry system that is permanently docked to a space station. It is designed to rescue individual space station crew or passengers when their lives are in danger due to catastrophic damage to a space station when there is no other Earth return transport available. As with the Pluto EAD concept, a passenger or crewmember is encapsulated and protected from entry conditions within the EAD envelope along with short-duration life support and a means to land on the surface after entry and post-entry separation from the pod. The system could be designed to be autonomous and continuously aware of its orbital location, achievable landing sites around the world, and atmospheric density conditions that could affect landing zone uncertainty.

Benefits. A Rescue Pod offers passenger or crew rescue capability without having to continuously dock transport spacecraft allowing transport spacecraft to be deployed in a cost-effective manner. Alternatively, it could be combined with already docked transport spacecraft, thus provides an additional level of redundancy for safety. A Rescue Pod also offers a way home in the event your ride is not available, e.g., when international politics intervene.

System Concept. Key Rescue Pod system components include 1) a 30 m diameter Enveloping Aerodynamic Decelerator (EAD) for entry and initial descent; 2) attitude control and de-orbit delta-V propulsion system, which is jettisoned after EAD deployment and inflation; 3) crew or passenger life support; and 4) a low-altitude (<50 km) deceleration and landing system. Pod payload mass is assumed to be 200 kg that includes the crewmember, their space suit, life support, and a deceleration and landing system. The total entry mass is about 350 kg. Additional capabilities and hardware could include an autonomous update of station orbit, landing sites and de-orbit phasing, and entry atmospheric density profiles; a space station attachment and separation system; a guided parafoil deceleration and landing to ensure landing in a safe location; communications radios and emergency locator beacons; and ground survivable gear. Assuming an International Space Station altitude of about 400 km, deorbit delta-V is less than 100 m/s, entry g-loads are less than 9 gees, and entry heating is less than half of that at Pluto or about 1.6 W/cm^2. The entry deceleration is about the same as for a Soyuz uncontrolled reentry; harsh, but entirely survivable. Time from the deorbit delta-V to entry is about 50 minutes.

4.7.2. Neutral Atmospheric Density Monitoring System

Knowledge of Earth's neutral density atmospheric density as a function of altitude and position on the Earth is useful for extrapolating the trajectories of spacecraft at low altitudes where drag has an appreciable effect on orbital decay. A small EAD can be used as a direct probe of this density.

There are both empirical and physics-based models to predict neutral densities in the lower ionosphere, thermosphere, and mesosphere (ITM) system; however, there are few measurements of these densities that can provide crucial atmospheric model validation and assimilation data for nowcasts and forecasts for low LEO altitudes. The result is that the density predictions in low Earth orbit have a high uncertainty due to uncertain atmospheric drag effects especially when the satellite orbit altitudes near Earth reentry leading to great uncertainty of the entry location and timing. GAC explored options to develop an EAD-based neutral atmospheric density monitoring system.

Problem. Interactions between the solar wind and the Earth's magnetic field during geomagnetic storms produced large short-term increases in upper atmosphere temperature and density can result

in increasing the drag on satellites, changing their orbits, and increasing the potential for satellite-to-satellite, hypervelocity collisions. This problem was highlighted by the recent loss of 40 Starlink satellites, that were literally pulled satellites out of orbit by drag.

System Concept. The Neutral Atmosphere Density Monitoring System concept is designed to provide multiple, affordable, and expendable thermosphere/mesosphere probes in a compact format that can be stored on space stations, like the International Space Station (ISS), and launched on demand. A single unit deploys into a lightweight satellite equipped with one or more accelerometers to directly measure drag effects, a GNSS receiver to provide precise orbit determination data, a ground radio link, and a passive deorbit system that enables prompt reentry after deployment from a space station. The system uses a spherical geometry to ensure an accurate coefficient of drag. System deployments will obtain acceleration and trajectory data during descent and reentry, enabling accurate neutral density profiles at very low altitudes for novel science investigations of the ITM system, forecast model data assimilation, and nowcasting data to inform launch operations.

Figure 31. Atmospheric Density Monitoring System just released and deployed from ISS.

Potential NASA Applications. NASA provides increased understanding of the physics of the Sun-Earth system through space-based observations and modeling, the development of new space-based space-weather technologies and missions and monitoring of space weather for NASA missions. This proposed system advances operational and space-weather science and technology by providing researchers data critical to the validation of physics-based, space-weather, atmosphere interaction models of space-weather events.

Other Applications. Other markets for this technology initially include NOAA and the DOD activities by providing data for space-weather assimilation applications that are desired by established space-weather operational organizations. All these benefits will provide commercial space organizations the data they need to operate their satellites, constellations, and private space stations efficiently and safely.

5 Enveloping Aerodynamic Decelerator (EAD) Development

In this section we discuss the EAD envelope design environments; the design driving envelope membrane stress; the thermal analysis and design; the envelope components design, fabrication and testing; and our EAD scale model envelope packing, deployment and inflation model.

5.1 EAD Envelope Design Environments

The EAD envelope design environments are shown in Table 5. The driving requirements are *High Heating*, *Peak Heating*, and *Peak Dynamic Pressure*. Figure 32 illustrates the EAD peak envelope entry conditions assuming a worst-case flight path angle and thermal model.

Table 5 EAD envelope design environments.

Event	Temperature, °C	Internal Pressure	Dynamic Pressure, Pa	External Pressure	Duration
Packing	20	<1 bar	0	1 Bar	days to weeks
Ground Storage	20	Vacuum	0	Vacuum	~1-2 years
Space Storage	20	Vacuum	0	Vacuum	10-12 years
Deployment	20	Vacuum	0	Vacuum	minutes
Inflation	20	62 Pa	0	Vacuum	minutes
Begin Entry	-100	58 Pa	0	Vacuum	minutes
High Heating	>400	>100 Pa	3-60	Vacuum	40 seconds
Peak Heating	600	158 Pa	37	Vacuum	1 second
Peak Dynamic Pressure	520	157 Pa	60	Vacuum	1 second
Lander Separation	-200	~15 Pa	0.2	~1 Pa	minutes

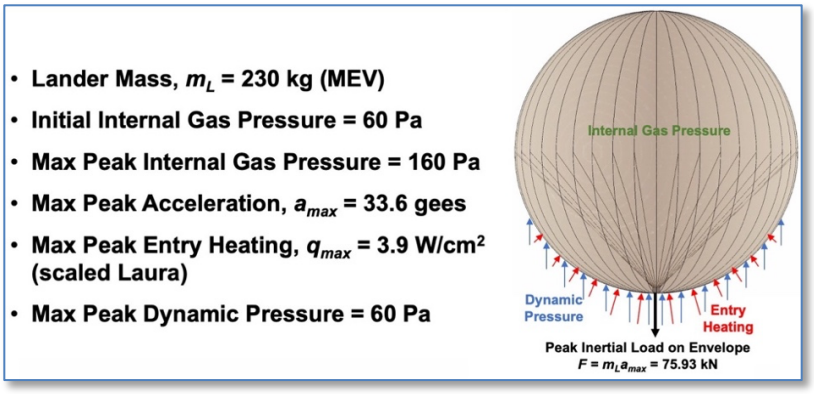

Figure 32 EAD peak envelope entry conditions.

It turns out that most of the membrane stress arises from the internal pressure; lander g-loads only adding about 10% more, and that only on the aft portion of the envelope since the lander loads are distributed into the envelope equator.

5.2 Driving Envelope Membrane Stress

The worst-case thermal model predicts the temperature of the helium in the envelope that can be used to calculate the internal envelope pressure. The envelope is filled with helium at inflation to an internal pressure of about 62 Pa. As the gas temperature increases during the entry, as shown in

Figure 36, the internal pressure increases to a maximum of almost 160 Pa at peak heating. Assuming a perfect gas, constant volume, and a uniform pressure and temperature of the gas, the pressure as a function of time from entry can be calculated and is displayed in Figure 33. The peak pressure occurs near at the peak heating point at about 135 s into the entry. This pressure can be used to calculate the peak stress load on the envelope. In addition, Figure 33 displays the dynamic pressure as a function of time through the entry. The internal pressure must be greater than the stagnation pressure to prevent envelope buckling and possible aerodynamic instabilities.

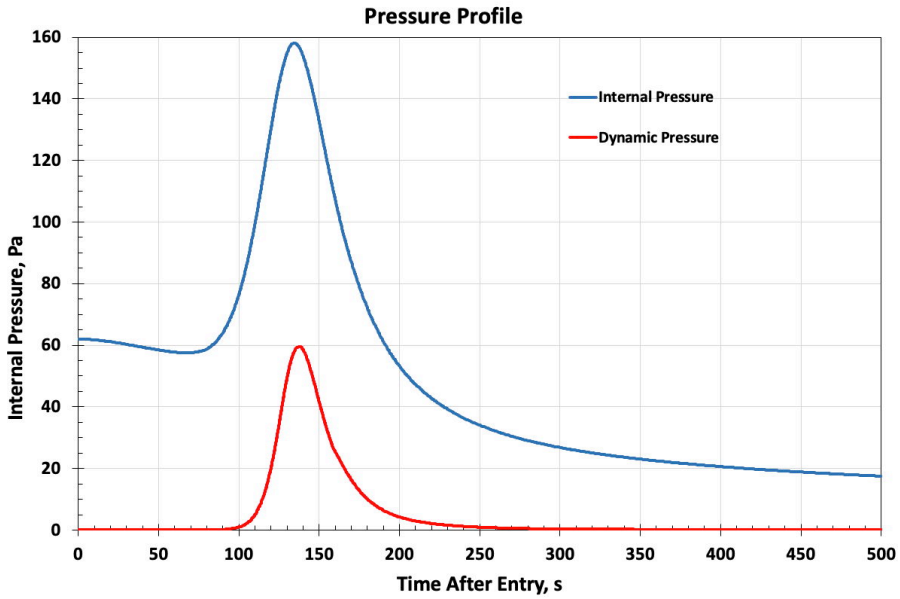

Figure 33 Envelope internal pressure profile from entry.

Given the maximum expected internal pressure in the envelope, the maximum pressure-induced membrane load in a 70-m sphere inflated can be computed and is about 2.8 kN/m. In addition to this membrane load, the envelope will see a distribution of dynamic pressure across its leading surface as well as applied load at its equator from the internal cords that support the decelerating lander. Locally, the dynamic pressure relieves load in the leading surface because it has the effect of reducing pressure difference across it. The 76 kN inertial load from the lander is distributed around the inside of the equator. The radially inward component of this load results in a small amount of radial inward deflection of the equator before it is reacted. The in-plane component of the inertial load is the greater component and is carried in-plane into the membrane material above the equator. For simplicity, we conservatively assume that the entire inertial load is added to the meridional membrane load above the equator. The design goal of the cord-envelope equator interface will be to uniformly distribute the cord loads into the envelope. This inertial load of the lander increases the membrane load on the aft hemisphere of the envelope by about 0.35 kN/m^2 to a total of about 3.1 kN/m^2; however, the aft hemisphere is at a much lower temperature. Figure 34 displays the worst-case envelope membrane stress profiles. The green curve is the stress at the equator caused by the lander g-loads that are distributed into the equator by load lines. The blue curve is the internal pressure stress profile stemming from the increase in internal pressure from the increase in inflation gas heating. Finally, the red curve is the total stress at the equator from both the inertial loads of the lander and the internal pressure. Note the peak stress with high temperature is just the internal pressure stress since the equator is 90° from the stagnation point heating.

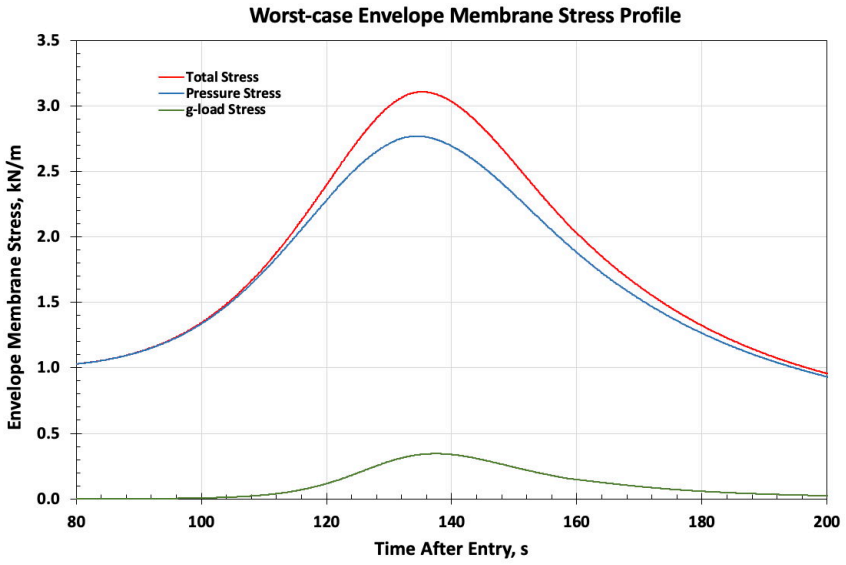

Figure 34 Worst-case envelope membrane stress profiles.

5.3 Thermal Analysis and Design

The EAD has a unique thermal design that does not require much, if any, thermal protection, since the envelope is so thin that entry heating is radiated away from both surfaces of the envelope skin to keep it cool. In addition, entry heat is transferred to the inflation gas by internal convection that also contributes to keeping envelope and seam temperatures low, thus eliminating the need for traditional TPS. This design strategy enables the use of commercially available films such as polyimides.

In Phase II, we have refined the one-dimensional thermal model developed in Phase I to estimate the worst-case envelope skin, seam, and internal gas temperatures during reentry. Key assumptions for the model are:

- Worst-case flight path angle (FPA) at entry of -65° at an altitude of 1600 km,
- Entry mass of 640 kg
- Front face envelope skin and seams are treated as two distinct lumped masses with uniform temperature across them,
- Seams are assumed to be 4 layers of laminate,
- Helium inflation gas is a lumped mass with uniform average temperature,
- Initial temperature for all components is 300 K,
- Envelope skin has zero transmissivity in the infra-red,
- Heat radiates from each face with a view factor of one,
- Emissivity of Kapton® film and of PBO is 0.9,
- Absorptivity is equal to the emissivity of each component, and
- Aerodynamics only directly heat the ram-facing side.

Figure 35 is a schematic that illustrates the thermal model physics.

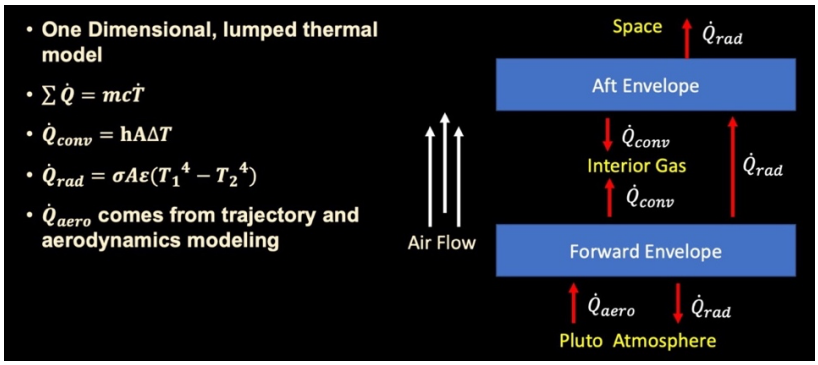

Figure 35 Thermal model physics.

The thermal model predicts component temperatures during reentry as shown in Figure 36.

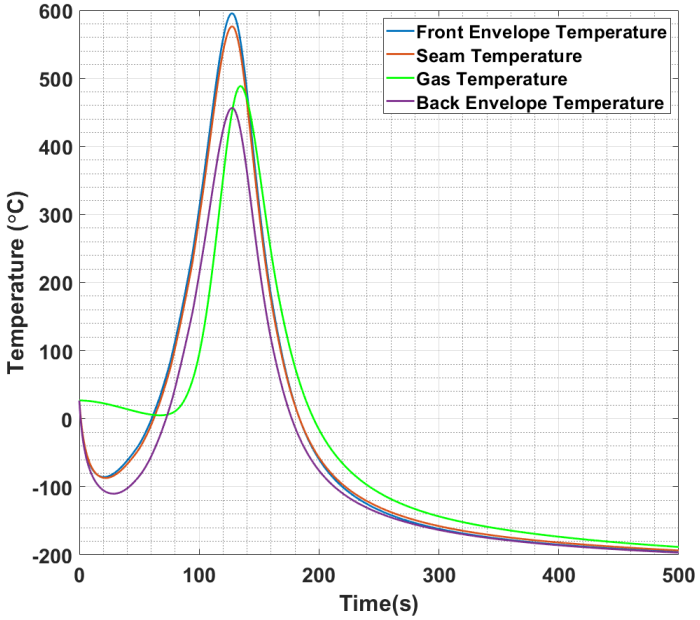

Figure 36. Envelope surface, seam, and gas temperatures during entry

The aerodynamic heating rate is estimated for a spacecraft with a 640 kg entry mass, 70m spherical envelope, and a -65º entry flight path angle at a 1600 km altitude. From the results of the mission analysis, the flight path angle is chosen to represent the worst-case heating. The thermal analysis shows that the ram-facing envelope surface and seams have a negligible temperature difference during entry. The model predicts a 600°C worst-case, peak surface temperature and a 40 second period when the envelope is above 400°C. This temperature is higher than the Phase I analysis; however, given previous testing of thin Kapton® films, we believe that this peak temperature, and its short duration of exposure, is acceptable for the design materials at entry.

In addition to estimating the temperatures near the stagnation point, we scaled results from LAURA, the NASA CFD code, results to estimate the heating rates and temperatures away from the stagnation point. In Figure 37, we show the scaled LAURA results for the stagnation point at θ equal to zero. We then scaled the LAURA results at higher values of θ.

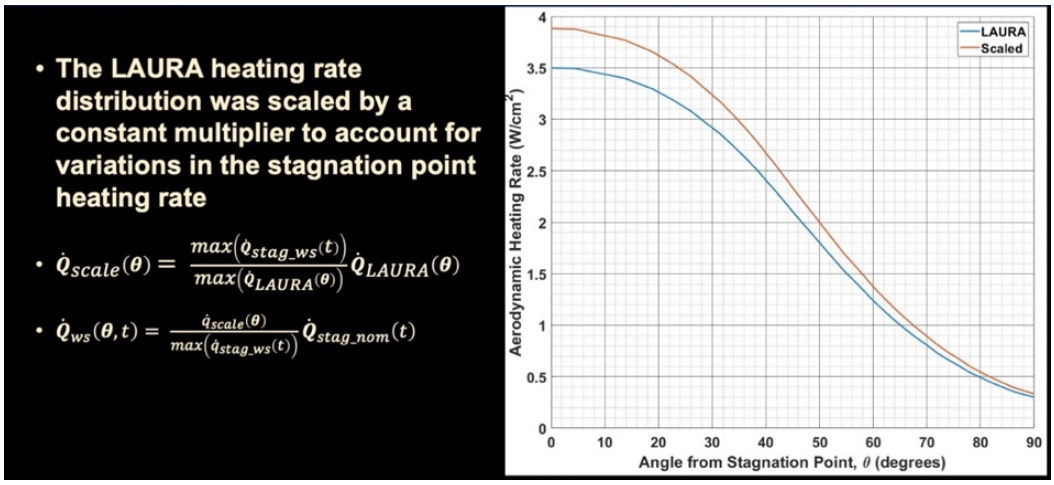

Figure 37 LAURA scaling.

We then calculated the temperatures of the front-facing envelope from the LAURA heating rate as shown in Figure 38. Since we know that the lowest peak temperatures, from the 1D model, are 460°C for the back film, we create an estimated temperature curve of the forward-facing hemisphere. This indicates a possibility of reducing yarn denier, and thus strength, in the envelope beyond θ of about 50°, which would result in a significant mass saving. A 2D thermal model is really needed here to validate these temperatures. We believe the 1D thermal model is conservative yielding higher temperatures than the envelope would see at entry.

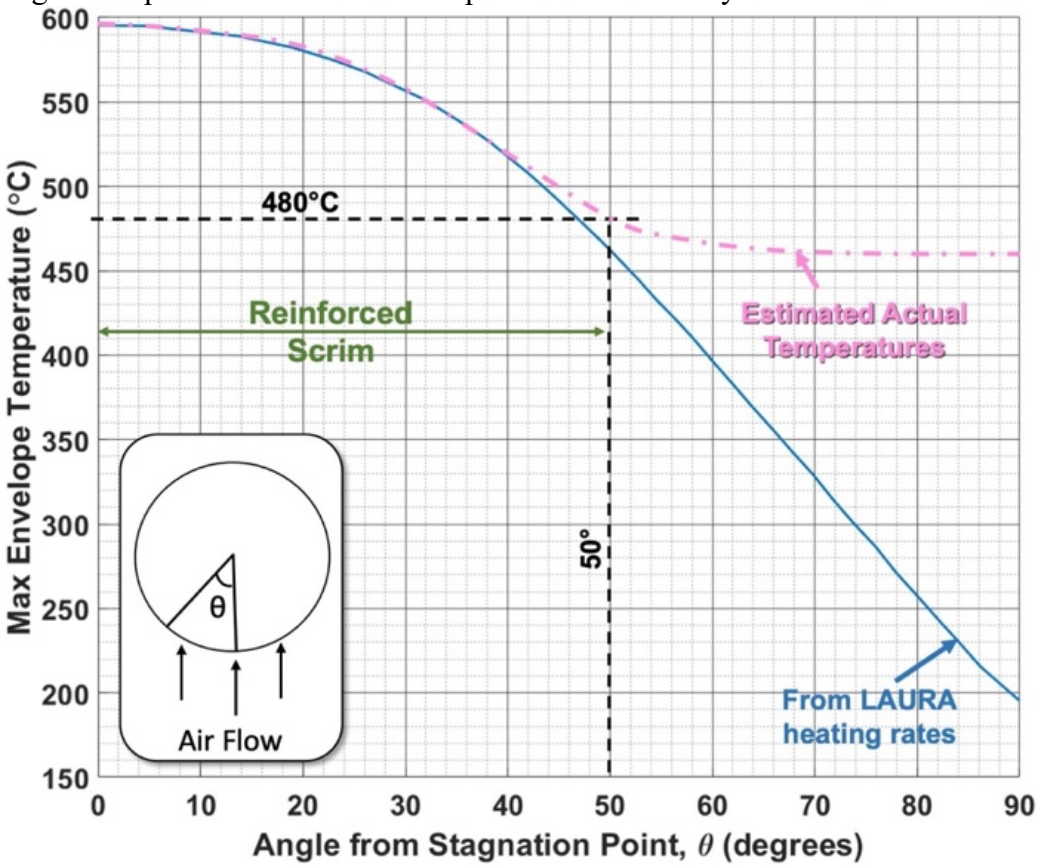

Figure 38 Temperatures vs. stagnation angle.

5.4 Envelope Design Summary

Figure 3 illustrates an envelope along with payload support lines. For the Pluto mission, the envelope is 70 m in diameter, masses 338 kg and is constructed of 96 gore sections. The gores are fabricated from a two-function composite made of an ultra-thin polyimide film laminated to a polybenzoxazole (PBO) scrim. The film acts as a gas barrier while the PBO scrim handles the deployment, internal pressure, and entry g-loads.

The scrim is a Leno weave with two different yarn deniers, a forward (ram-facing) region and an aft region (wake-facing). The yarn spacing is about 1 cm. Load lines within the envelope distribute the deceleration loads of the lander into the EAD envelope equator via a lightweight, fabric interface, which reduces loads in the ram-facing portion of the envelope where there is higher heating. The load lines also help keep the envelope shape spherical at the windward end of the EAD.

The envelope gas barrier a Kapton® film 7.6 μm thick. The strength member is a scrim composed of 250 denier (forward sectors) and 100 denier (aft sectors) Polybenzoxazole (PBO) yarn pairs. The non-seam envelope areal density estimate is about 20 g/m^2. The envelope made of 96 gore assemblies that each are made of several gore segments all seamed together. The lander payload is supported by Kevlar® load lines tied to an equatorial Nomex® fabric catenary curtain. There is a forward-facing closeout feature to enclose and allow release of lander after entry. Finally, there are gore design features to facilitate fabrication and assembly of the envelope to the ram-facing, forward support structure and the wake-facing envelope endcap.

5.5 Envelope Components Design, Fabrication, and Testing

In this section we discuss the envelope materials, the scrim and laminate design and fabrication, the design of seams, and the testing of these components. We began to introduce the testing program of the component materials that was undertaken. We worked with Oklahoma State University (OSU) and our softgoods consultant, Jody Ware, on the design of the envelope and the thermal and stress testing we need to do to validate the envelope design.

5.5.1. PBO Protection

PBO, a high modulus, high tenacity yarn, is well-known to have performance loss with exposure to light, primarily the UV component, and humidity. To reduce this risk, the PBO yarn stores at GAC were placed in sealed, opaque black bags along with packages of desiccant. Both OSU and the scrim vendor were apprised of the issues with PBO exposure to light and humidity and made sure PBO yarn was kept in sealed, dry packaging and to reduce light exposure when processing components with PBO. When weaving PBO yarns into scrim, the manufacturer was required to cover the work product with opaque shields during breaks in weaving. That being said, while exposure to light and humidity was minimized it could never be eliminated completely. In addition, when selecting bonding agents that would contact PBO, we expressly review the potential detrimental effects of the bonding agent on PBO.

5.5.2. Scrim Design and Fabrication

The scrim was a Leno weave as illustrated in left of Figure 39 constructed of 250 denier PBO yarns. In the fill direction, two 250 denier yarn pairs are twisted together for added strength. In the warp direction, each 250-denier yarn is woven about the two yarn pairs in the fill direction. The

yarn spacing is about 2.7 yarns per inch. The initial production run for laminate fabrication and testing was about 18 inches wide. The image to the right of Figure 39 is an example of the production scrim. As discussed above, the PBO yarn denier would change depending on the location on the envelope. One uncertainty is the possibility of damage to the PBO during the weaving process. The woven yarns were never mechanically tested for breaking strength after weaving and prior to lamination, due to the looseness (instability) of the unsupported weave.

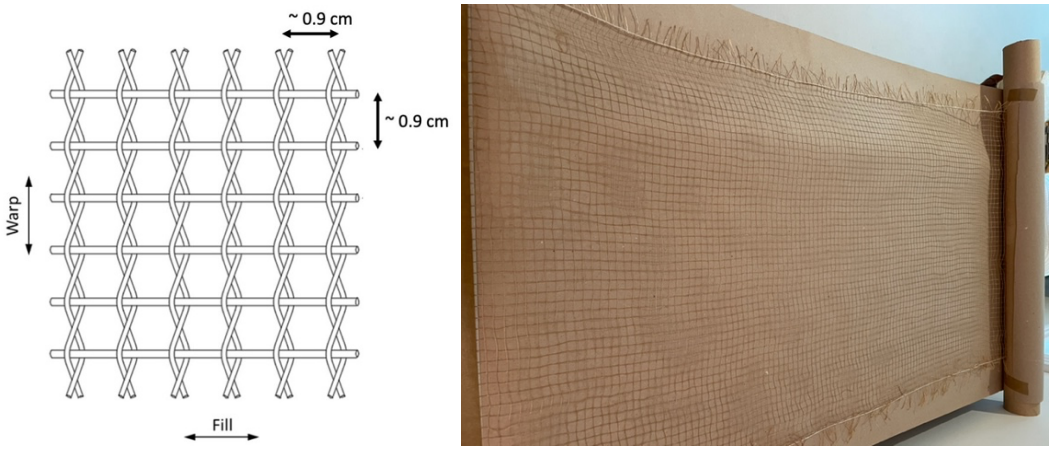

Figure 39 EAD envelope PBO scrim design.

5.5.3. Laminate Design and Fabrication

The envelope is a composite of the Kapton® film and the PBO scrim. The intended configuration for use in the objective unit is with the scrim facing outward, and the Kapton gas barrier facing inward. For performance testing the initial laminate fabrication experiments used some of the pre-production scrim and were typically sized for the experiments to be 16 in by 16 in. The scrim was bonded to the film using an epoxy. A fixture was used by OSU to hold the scrim in place while it was coated with epoxy using a roller. Then a sheet of 0.3 mil Kapton® film was attached to the scrim and the entire laminate held in place by means of vacuum pressure overnight after which the epoxy underwent curing at 200°F for two hours. Figure 40 illustrates the vacuum curing process on the left and the final laminate on the right.

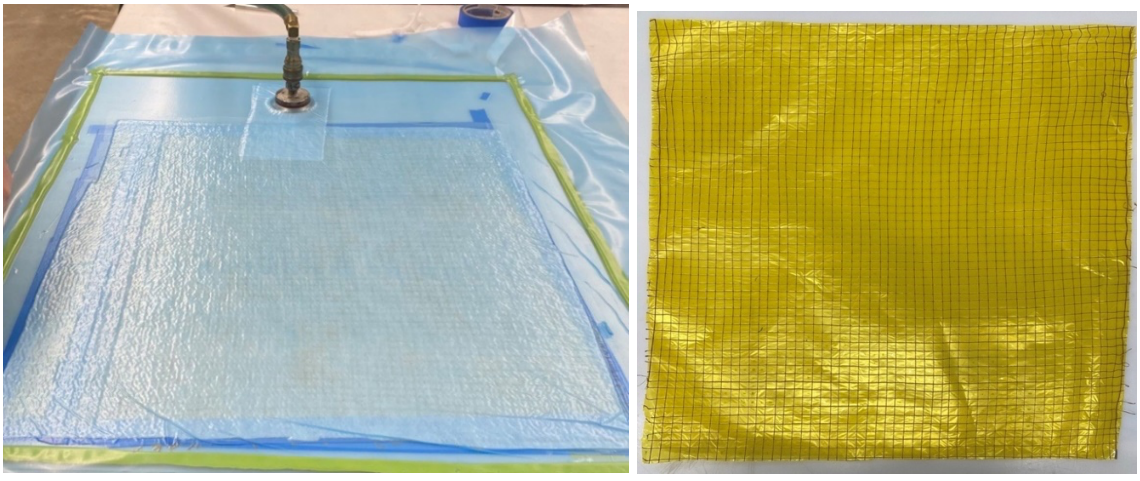

Figure 40 Laminate fabrication.

As discussed above, worst-case peak envelope temperatures about 600°C are expected on the forward-facing envelope for a few seconds during entry. We designed a fixture to conduct seam testing with the Instron machine at temperature and within a nitrogen envelope. A xenon lamp heater would heat the sample at 600°C per minute after which we would pull to break. While we initially planned to conduct seam strength testing at temperature, fabricating the heater apparatus was considered too challenging given the limited funding available. This testing will be planned in a later effort.

However, we did test the PBO scrim and Kapton® film strength at temperature that allows us to estimate seam strength at temperature. We also performed room-temperature testing of unseamed laminate and seamed laminates to understand the loads that can be tolerated by the designs. Finally, we tested bare PBO yarn at 600°C at heating rates of about 600°C/minute.

As discussed earlier, the envelope is a composite made from a 0.3 mil Kapton® film bonded to a PBO scrim. The scrim is fabricated from PBO yarn as a leno weave of about a 1 cm grid spacing. We plan to fabricate the film/scrim laminate composite material; construct sample gore seams from it; and conduct realistic laboratory tests of the composite and seam samples.

5.5.4. Laminate and PBO Yarn Testing at Temperature

Figure 41 illustrates the objective heating rate profile with a seam temperature increase from 20°C, around room temperature (RT), to 600°C in about a minute followed by a similar, but opposite cooling rate. In actuality, the membrane stress follows the gas temperature profile that lags the envelope temperature by about 7 s, which means that when the peak temperature is experienced by the envelope, the membrane stress is a little lower, by about 0.143 kN, than at its peak of 2.768 kN.

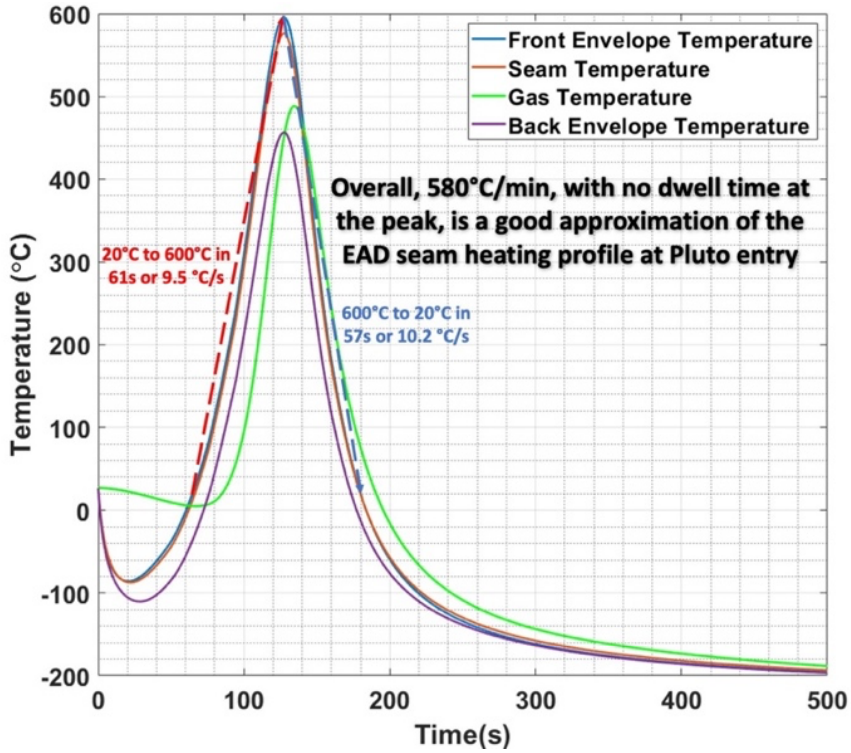

Figure 41 Objective heating rate profile.

The objective was to conduct narrow sections of laminate and PBO yarns at high rates of heating corresponding to 600°C per minute temperature increase rate and be able to determine strength at a temperature of 600°C.

A fixture was constructed by OSU to perform laminate sample and bare PBO yarn heating at high rates while a deadweight was attached to the yarn. The goal was to reach the peak temperature of 600°C and peak tensile load in about 1 minute. OSU completed testing of narrow laminate samples at high temperature.

Test Apparatus Design Specifications. Allow an operator to apply a deadweight on a sample and heat it at a controlled heating rate to measure the breaking time (and temperature of the sample environment at the breaking time). Enable the heating rate and its profile (linear vs. nonlinear) to be adjusted. The deadweight discrete loading range from 20 to 120 N with a load step of 5±0.5 N. No slippage of the grip. Sample dimensions of ≤2cm wide by 95 cm long. Heating rate ≤ 750 ℃/min.

Test Apparatus Design. Oxyfuel (propane and air mixture) combustion was devised to heat the samples utilizing a combination of radiation and convection heating mechanisms. In addition, a flow regulator can adjust the propane flow rate. Safety features were devised to keep the heating source away from the propane tank using an extension hose at the bottom side of the heat reflector, preventing the rise of the hose temperature. Also, a funnel was devised and installed on the burner opening to concentrate the heating flow and limit the radiation area to the flame-resistant ceramic shield, which involves an aperture to direct the heating energy on the sample surface. Using a linear stage driven by a stepper motor and gearbox, the speed of the burner and its distance from the ceramic shield can be controlled. Further improvement can be made to include a closed-loop system to automatically control the speed and location of the burner in order to increase the accuracy of the heating rate profile.

The apparatus involves top and bottom ceramic shields to prevent heating the grips. Also, an exhaust canopy was installed to lead the byproduct fumes out of the test room. Deadweight was applied using a hanging basket on the bottom grip. Figure 42 shows the schematic of the apparatus with all design features. In Figure 43, a picture of the middle part of the apparatus is shown.

For experiments, two people (preferably three) are required to control the burner motion, temperature measurement, and video recording and turn off the burner at the end of the experiment (breaking).

Temperature Measurement. A K-type thermocouple was used to measure the temperature of the air at distances from the opening of the burner. Air temperature depends on the propane gas flow and gas-to-air ratio. It was confirmed that the temperature is almost constant with a tolerance of ±10 ℃ at a distance from the burner opening. Figure 44 shows temperature measurements at different distances from the burner opening under a constant propane gas flow and environmental parameters (room temperature and humidity). Each data point is the average of three measurements obtained in a 20 mm wide band perpendicular to the top half area of the burner opening at each distance. Figure 44 also shows a schematic of the temperature measurement spots where a laminate sample could be held in front of the ceramic shield aperture in front of the burner opening. The data in Figure 44 was used to calculate the burner's speed during the heating process to obtain a heating rate of 600 ℃/min for the air. Assuming the sample temperature will be the same as the air temperature at a specific distance from the burner opening, different speeds were devised for the burner motion toward the ceramic shield aperture to have the desired heating rate of 600

°C/min. Figure 44 shows the heating rate of the three spots in the air where the sample center and edges will be located during the test. Figure 46 shows the heating profile of the air where the bare yarns were located for measuring their load-carrying capacity under the heating rate of 600 °C/min.

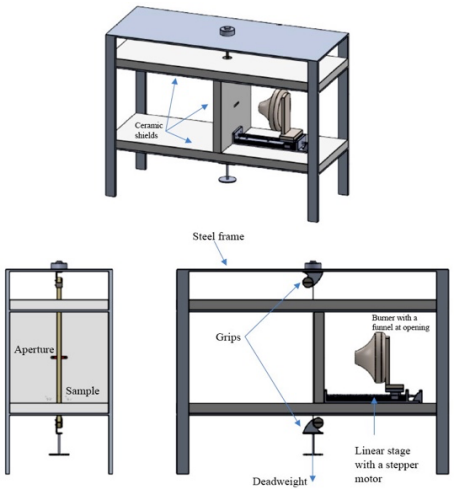

Figure 42 Schematic of narrow laminate and yarn test apparatus.

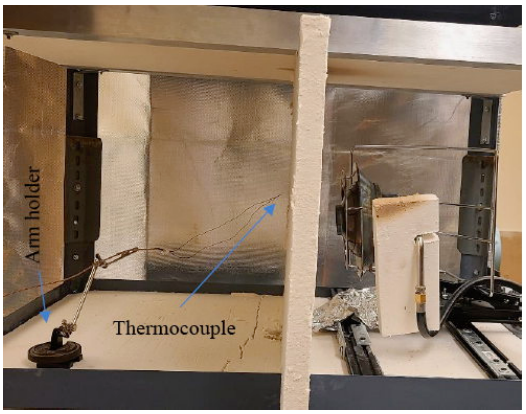

Figure 43 Narrow laminate and yarn test apparatus.

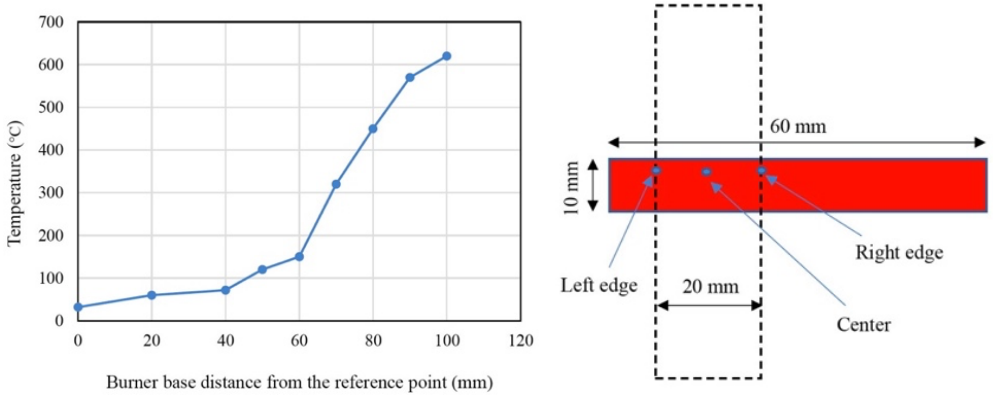

Figure 44 Temperature measurements at different distances from the burner opening (left), Schematic of the temperature measurement spots where the laminate sample or yarn will be held in front of the ceramic shield aperture (right).

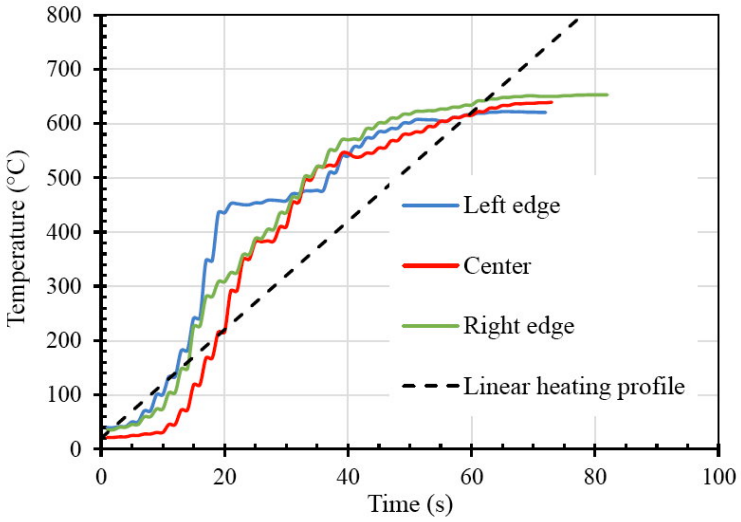

Figure 45 Heating rate of the three spots in the air, shown in Figure 44, where the sample center and edges were located during the test.

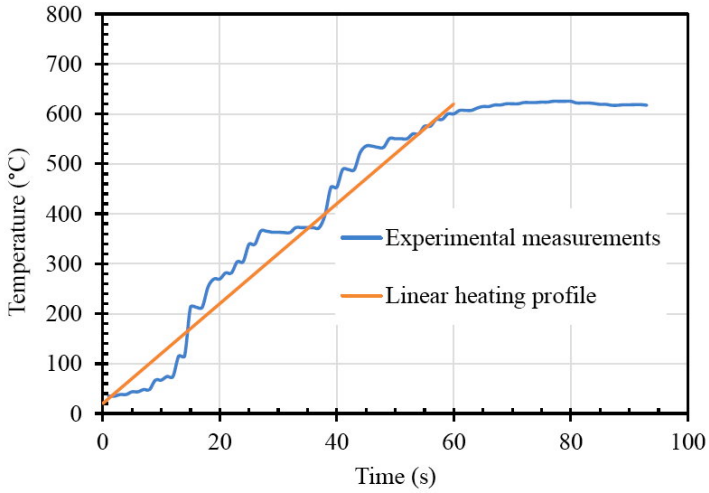

Figure 46 Heating profile of the air where the bare yarns are to be located during their tensile tests.

Two concerns with this setup are that the temperature measurement was made of air by a bare thermocouple, not a PBO yarn temperature. Due to differences in thermo-optical properties of the thermocouple and the PBO, there could be different actual temperatures of the PBO exposed to the burner. Another concern is that the test was done in air and employed a propane burner that could cause increased sample oxidation damage than if the heating was caused by nitrogen gas (Pluto atmosphere) heating.

5.5.5. Envelope Seam Design, Fabrication and Testing

Gore seam samples were initially stitched to ensure a load-bearing seam. Figure 47 illustrates two example stitching options that were initially proposed. As this initial work proceeded, we found that a desirable approach was to not use any bonding agents in the seam, since they added

considerable mass, but instead to use an overlapping and folded seam design with features to ensure capturing the loose scrim weave to facilitate load transfer across seams.

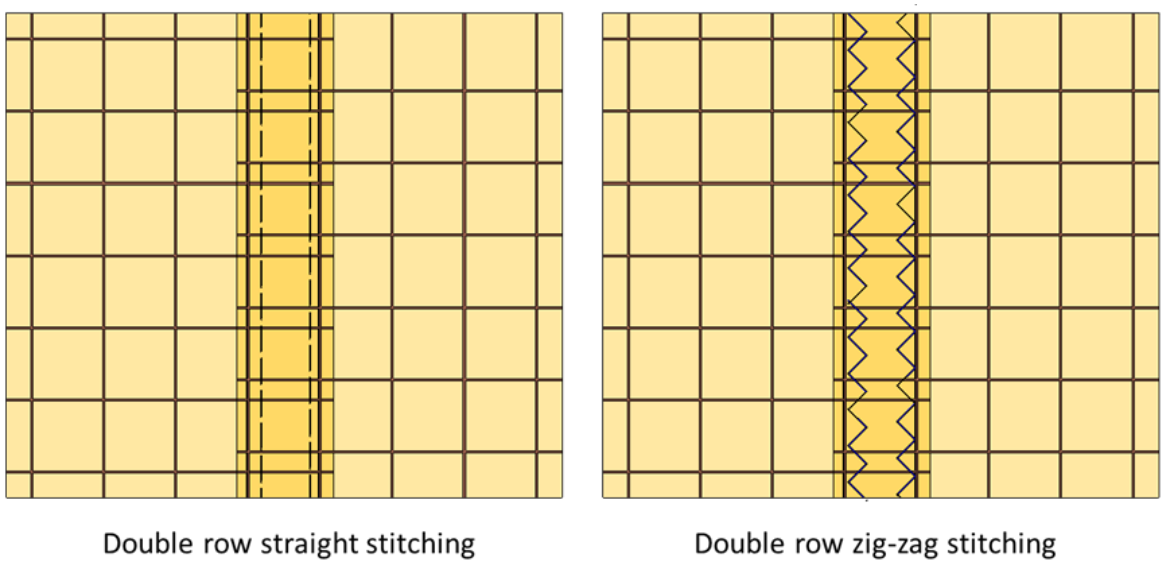

Figure 47 Two example seam stitching options

Seam testing was done in the usual tensile testing apparatus, i.e., Instron 5984 machine. Considerable effort was expended on Instron grip design to ensure the laminate would be loaded evenly. Testing of the overlapped and folded seams resulted in much lower strength than estimated since the seam is only cinched during the loading process, which fails the Kapton gas barrier. In addition, the strength of the seam was only a fraction of the base laminate.

We performed several bonding experiments of virgin PBO yarn to yarn and with scrim cross-machine direction (twisted yarn pairs) yarn to yarn samples with and without a Kapton® film substrate. Finally, we fabricated and tested seams in the laminate.

5.6 Scale Model Packing, Deployment, and Inflation Model

After a 10-plus year interplanetary cruise to Pluto, it is critically important that the EAD envelope be reliably deployed. Packing, deployment, and inflation of any space inflatable structure can be a challenge, but the lessons learned in the NASA Echo Project point to solutions. It is important to avoid deploying too quickly since that could damage a very thin envelope. Even small quantities of gas trapped inside the stowed envelope will keep accelerating the film outward in space since there is essentially no external pressure resisting the motion. However, it is essentially impossible to remove all the trapped air when packing the envelope on the Earth. One approach used by the Echo project was intentionally to add many tiny vent holes all over the surface of the envelope film. Once in the hard vacuum of space, this provided the ability for residual gasses to vent before adding inflatant in a slow manner during inflation.

There are several ways to inflate the envelope including using gas, such as helium, stored in high-pressure vessels; subliming solids, as employed in the NASA Echo balloon projects of the 1960s; vaporizing liquids, or gas trapped in the folds of the envelope under storage if that can be controlled. Regarding small payloads for Earth reentry, one or more subliming solids can effectively inflate an envelope only using the heat of vaporization of the solid, which can be quite low. One inflation idea is to include a small amount of subliming solid sprinkled throughout the

envelope so that when deployed gas will partially fill the envelope providing pathways for the main helium inflation gas.

5.6.1. Scale-model Envelope Design

Our teammates at the Unmanned Systems Research Institute (USRI) OSU have designed and fabricated a 1/20th scale packing and deployment model. This model was fabricated from 12-gore, 0.3 mil, high-density, polyethene film to study and test folding methods and deployment strategies to gain insight into the deployment and inflation mechanics and to develop a viable packing concept. This scale model included internal load lines for system fidelity. Figure 48 is a drawing of the 1/20th scale model and Figure 49 are pictures of the desktop practice models that were used to develop fabrication concepts.

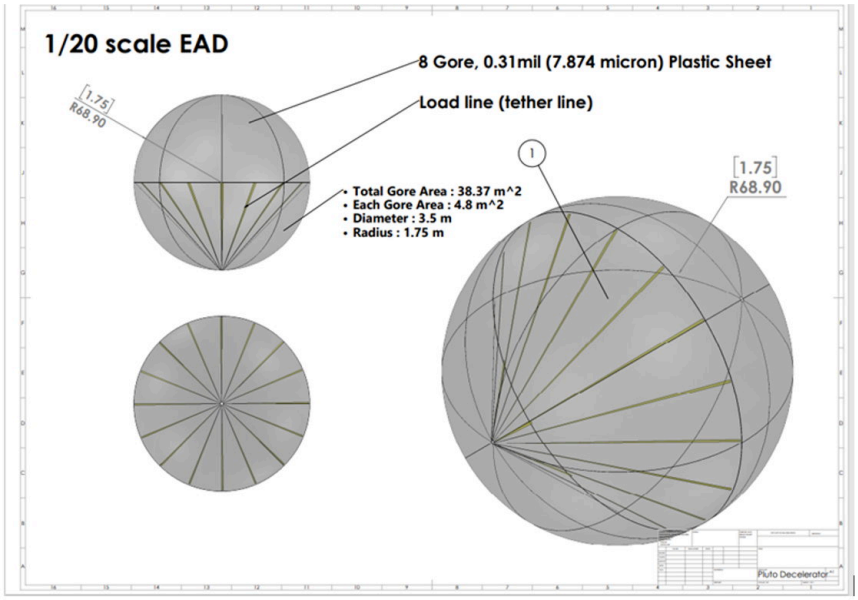

Figure 48 1/20th scale model Pluto EAD drawing

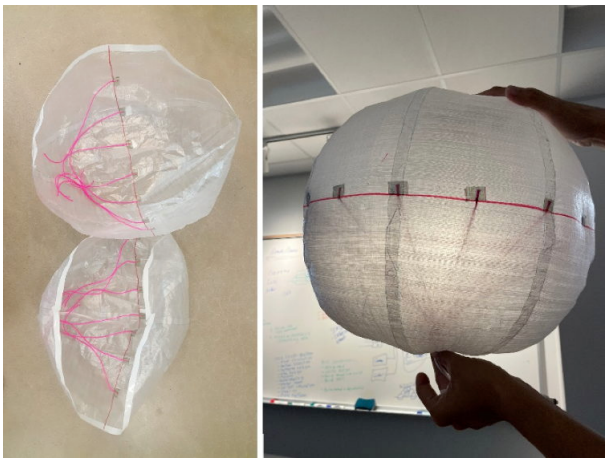

Figure 49 Desktop fabrication scale models

The envelope diameter was 3.5 m with an area of 38.4 m^2. Table 6 shows the 1/20th scale model material options considered along with the selected choice of material. Given the Option 2

envelope film selected for the packing build, the total mass of the 1/20th scale model was about 650 g.

Table 6 Scale Model Material Options.

1/20 Model: Fabric Option and Selection for Gore

Area Density (Light to Heavy)

Goal: Transparent and lightweight

	Option 1	Option 2	Option 3	Option 3	Option 5	Option 6
Parameters	Kapton* 30EN 0.29 mil	HDPE Sheeting 0.31 mil	HDPE Sheeting 1.0 mil	UHMWPE (Dyneema) CT1	HDPE Sheeting 1.5mil	UHMWPE CT5
Area Density (g/m^2)	1.1	7.2	23.2	25	33.75	50
Thickness (mm)	0.0075	0.008	0.025	0.03	0.038	0.085
Rigid (handling)	Yes	No, can tear easily	No	Yes	No	Yes
Bonding Type	PSA??	Packaging Tape, Head sealing (burn risk)	Packaging Tape, Head sealing (burn risk)	PSA tape, Sewing	Packaging Tape, Head sealing (burn risk)	PSA Tape, Sewing
Cost and size	?? And size?	$0.239/yard (12 ft wide roll)	$0.77/yard (9 ft wide roll)	$34/yard (4.5 ft wide roll)	$2.61/yard (50 ft wide roll)	$49.8 /yard (54 in wide roll)

5.6.2. Scale Model Fabrication

After selection of materials, several scale models were fabricated. Some models were fabricated from 1 mil thick high-density polyethylene (HDPE) film to work out the fabrication procedures followed by fabrication of several scale models made from 0.3 mil HDPE film.

Initially, a template was laser-cut from thick paper from which all the envelope gores were cut. There was a four-step process for gore fabrication as illustrated in Figure 50. Step 1 - starts with a single layer of plastic sheeting; Step 2 - fold over to form a double layer sheet; Step 3 - fold over again to form a four layer sheet from which a gore shape is cut using the template; and Step 4 - unfold the full gore shape.

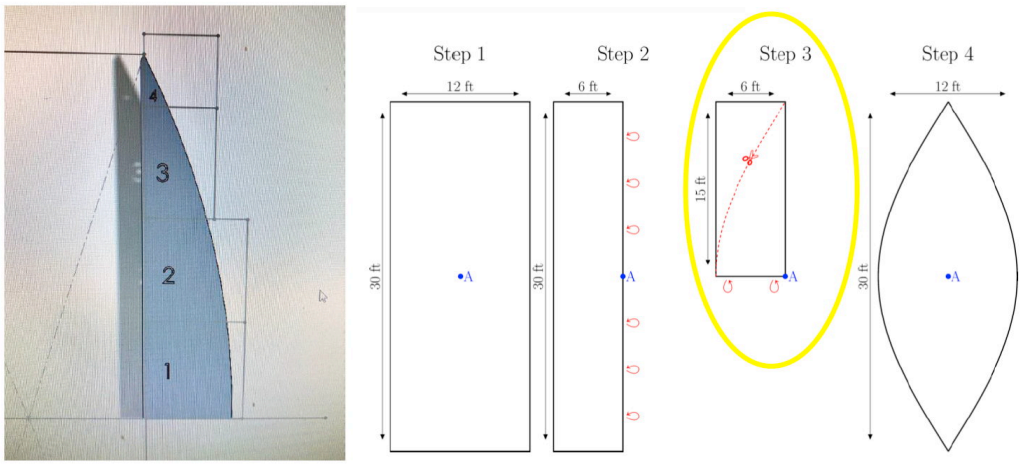

Figure 50 Gore template and fabrication

Gore templates were created from which gores were cut from the sheeting while it lay of the floor. The gores were then seamed together by use of 1-inch-wide double-sided adhesive tape. Gores

were bonded together in sets of two. This was followed by attaching load-line simulants. A fluorescent orange nylon yarn was selected for the EAD load line simulants. Next a 3-step zig-zag stitch was used to attach load lines to a CT5 Dyneema patch with pressure sensitive adhesive (PSA). Then each line was attached to EAD model by sticking them to the inside of each gore. Then all gore sets were bonded together leaving one end slightly open for simulated lander attachment. Figure 51 shows the scale model undergoing fabrication by OSU students.

Figure 51 1/20th scale model fabrication.

Figure 52 are photos of the initial 1/20th scale model EAD at OSU. This envelope is about 3.5 m in diameter, made from 1 mil high-density, polyethylene (HDPE) film, and has 12 gores. These preliminary scale models show the attachment of the load line simulants, red yarns, to the gore versus the seam. Later versions will have the attachment points be at the gore seam from strength.

Figure 52 Initial 1.0 mil thick 1/20th scale model Pluto EAD

The next model fabricated was made from 0.3 mil HDPE film. Two models were built including one fabricated by a Senior Capstone Design Team that is shown in Figure 53.

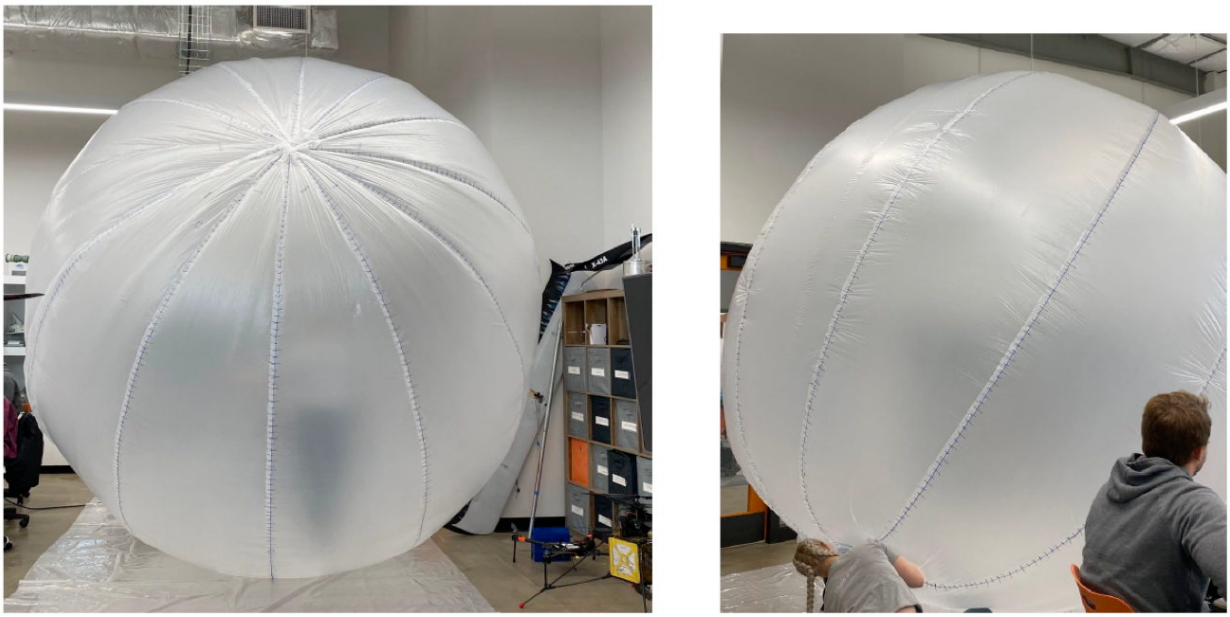

Figure 53 0.3 mil thick 1/20th scale model Pluto EAD

5.6.3. Scale Model Endcaps

Figure 54 illustrates the design and fabrication of the scale model end cap. Next, the end cap was attached to apex of EAD model for support. A deflation flap was designed and attach to the scale model. A circular plate was created for load line attachment after which load lines were tied to circular thin plate on which a simulated lander could be attached.

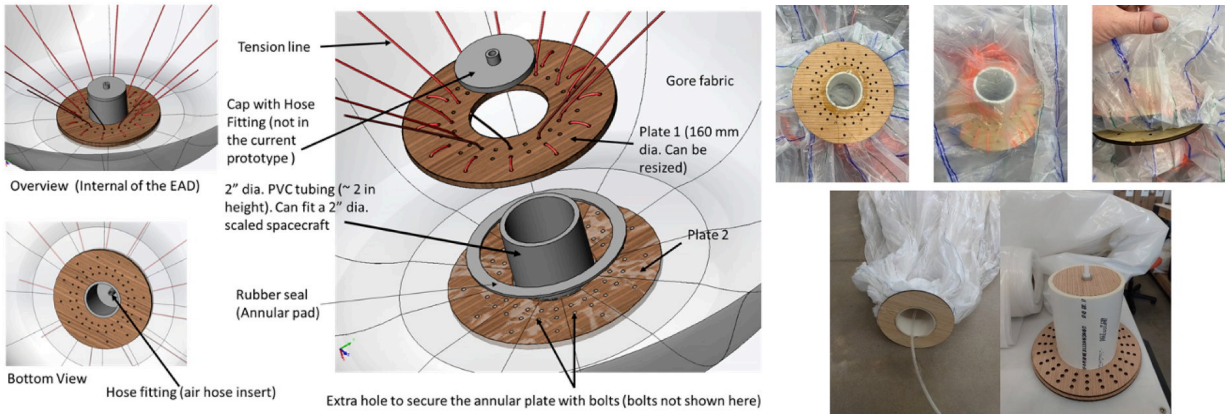

Figure 54 Scale model end cap design and fabrication.

5.6.4. Scale Model Packing Tests

Packing and deployment experiments were conducted to develop concepts that could be employed for a Pluto EDL mission A series of packing tests were performed at OSU on an EAD model of 3.5 m diameter made of 1mil thick HPDE plastic sheeting. Table 7 shows the packing test goal for the 1 mil scale model envelope. Much progress was made on packing testing, though the goal was not met before higher priority tasks needed to be performed. Next steps would be to conduct envelope folding on a large table and to incrementally mechanically press the envelope into a packing container, which might require a sturdy container and a hydraulic press.

Table 7 Packed Model Parameters for Packing Factor of 3.

Packed volume of	Model Envelope		For 1mil plastic EAD model		
Height	0.15	m	Scaled to pipe size	5.90551181	in
R_outer	0.1	m		3.93700787	in
V_outer	0.004712	m^3			
R_inner	0.055	m		2.16535433	
V_inner	0.001425	m^3			
Volume pf Packed Envelope	0.003287	m^3			
	3.2869	L	GOAL		

Figure 55 shows the results of initial packing tests with the 1 mil scale model envelope.

Figure 55 Scale model packing tests.

6 Reporting

The key reporting during this Phase II effort is listed below.

- August 10, 2021: Presented a paper on the concept at the International Planetary Probe Workshop (IPPW) in the Future Missions session,
- September 21, 2021: Presented the concept at the NIAC Symposium,
- January 4, 2022: Gave a briefing and published a paper on the concept at the AIAA SciTech Conference,
- January 24, 2022: Submitted a Quarterly Status Report to the NIAC Program Office,
- April 16, 2022: Submitted an Annual Performance/Progress Report to the NIAC Program Office,
- September 20, 2022: Presented the concept at the NIAC Symposium,
- October 4, 2022: NIAC Phase II Continuation Review,
- February 16, 2023: Briefing to Dr. Carolyn Mercer, Chief Technologist, NASA Science Mission Directorate (SMD),
- February 21, 2023: Published an article on *Mission Analysis for Landing on Pluto from a Fast, Hyperbolic Trajectory* in the AIAA Journal of Spacecraft and Rockets,
- March 6, 2023: Briefing to Michelle Munk, NASA STMD EDL Technologist,
- March 13, 2023: Briefing to Michael Wright, NASA STMD EDL Technologist,
- May 3, 2023: *Lightning Talk* on Concept to NASA Outer Planets Analysis Group (OPAG),

In addition, a news article was published by Jamie Carter for Forbes in May 2021 that included the Pluto Hop, Skip, and Jump concept.

7 Summary

An Enveloping Aerodynamic Decelerator (EAD) offers a compact, low-mass, and payload protection option for atmospheric entry and landing at Pluto and Neptune's moon, Triton.

Initial exploratory studies point to possible lander science measurements that could help address high-priority Pluto science themes of the past Decadal Survey and proposed strawman science packages have been documented.

Three key challenges were identified include successfully targeting and landing on Pluto; packing, deploying, and inflating the EAD prior to entry; and envelope seam strength at peak heating and g-loads. These challenges have been addressed.

A Monte Carlo landing uncertainty analysis was completed that incorporated approach orbit determination errors, entry system uncertainties, and uncertainty in the Pluto atmospheric density. Based on this analysis, we have demonstrated that an EAD-based entry and landing system can feasibly land on Pluto even in conservative levels of uncertainty.

The possibility of a Triton lander mission enabled by an EAD entry and lander system has been addressed and two modes analyzed, namely direct entry and orbiter delivered landers.

Began the development of two new EAD application spin-offs including a space station crew rescue pod and a neutral atmospheric density monitoring system.

We completed initial study of employing Solar Electric Propulsion (SEP) combined with multiple Earth-Venus gravity assists to enabled missions to Pluto and Neptune without needing to wait for Jupiter gravity assists.

We fabricated several scale model EAD envelopes for packing, deployment, and inflation experiments and we have begun packing experiments.

We also conducted a refinement of the envelope thermal analysis for envelope, seam, and inflation gas temperatures. Our thermal analysis and previous polyimide film testing indicate that there is a very good potential for Kapton® film as the EAD gas barrier.

We completed the analysis of the membrane stress on the envelope during peak heating and inertial loading.

We fabricated EAD envelope laminates and conducted stress testing at room temperature.

We patterned the envelope gore seams and using the thermal testing and analysis in the design of the seams destined for thermal and strength validation testing planned in a future effort.

We developed and used an experiment to extend knowledge of the strength of EAD laminate and PBO yarn at high temperatures (>500°C).

We fabricated two seam design options and tested them at room temperature and concluded that bonded seams will likely offer superior performance over stitched seams. In addition, we have concluded that future strength testing measurements should include scale model envelopes in order to increase material length. A greater length will allow greater equalization of the load in separate yarns.

Finally, we briefed key NASA STMD EDL technologists, the SMD Chief Technologist, and the Outer Planet Assessment Group (OPAG) on the NIAC Pluto Hop, Skip, and Jump concept project and the ability of EAD to enable entry, descent and landing on Pluto and bodies with tenuous atmospheres.